THE JOURNAL OF COMPARATIVE NEUROLOGY 460:345–367 (2003)

Chemical Anatomy of the Human Ventral Striatum and Adjacent Basal Forebrain Structures

LUCÍA PRENSA,[1,2] SANDRA RICHARD,[1] AND ANDRÉ PARENT[1]*
[1]Centre de Recherche, Université Laval Robert-Giffard, Beauport, Québec G1J 2G3, Canada
[2]Departamento de Anatomía, Facultad de Medicina, Universidad de Navarra, 31008 Pamplona, Spain

ABSTRACT

Calbindin D-28k (CB), calretinin (CR), substance P (SP), limbic system-associated membrane protein (LAMP), choline acetyltransferase (ChAT), and acetylcholinesterase (AChE) were used as chemical markers to investigate the organization of the ventral striatum (VST) and adjacent structures in healthy human individuals. No clear boundary could be established between the dorsal striatum and the VST, and the core/shell subdivisions of nucleus accumbens (Acb) could be distinguished only at the midrostrocaudal level of the VST. The CB-poor shell displayed intense immunostaining for SP and CR but only weak staining for LAMP. By contrast, the core was weakly stained for SP and CR and moderately stained for LAMP and CB. There was no difference between shell and core with regard to the cholinergic markers. The Acb harbored numerous ChAT- and CR-immunoreactive cell bodies, the latter being distributed according to a marked, mediolaterally increasing gradient. The size of the ChAT- and CR-immunoreactive perikarya in the Acb varied according to their location in the core and shell. The VST was surrounded by a chemically heterogeneous group of cell clusters referred to as *interface islands*. The CR-rich caudal portion of the VST merged with the bed nucleus of the stria terminalis dorsally and the diagonal band of Broca ventromedially, the latter two structures displaying complex immunostaining patterns. The claustrum was markedly enriched in LAMP and harbored different types of CR- and CB-immunopositive neurons. These results demonstrate that the neurochemical organization of the human VST is strikingly complex and exhibits a greater heterogeneity than the dorsal striatum. J. Comp. Neurol. 460:345–367, 2003.

Indexing terms: basal ganglia; basal forebrain; nucleus accumbens; striatal chemospecific neurons; interface islands; claustrum

Originally, the ventral striatum (VST) concept was intended to embrace the part of the striatal complex that receives afferents from allocortical areas rather than the neocortex (Heimer and Wilson, 1975). Hence, based on their afferents from the piriform cortex, the ventromedial part of the caudate nucleus and putamen, the nucleus accumbens (Acb), and the olfactory tubercle were all included in the VST concept. Although functionally very helpful, the VST concept remains a rather elusive anatomical entity, particularly for primates. For example, some authors have advocated that the human VST is limited to the Acb, its major component, and the surrounding ring of cell islands, also named *insulae terminalis* by Sanides (1957). However, it has been argued that, on the basis of its connectivity, the VST should include ventrally located parts of the putamen and caudate nucleus (Haber et al., 1990; Heimer et al., 1999).

The Acb is considered the major component of the VST. Together with neighboring sectors of caudate nucleus and

Grant sponsor: Canadian Institutes for Health Research; Grant number 5781; Grant sponsor: Fundación Marcelino Botín.

*Correspondence to: André Parent, Centre de Recherche Université Laval Robert-Giffard, 2601 de la Canardière, Local F-6500a, Beauport, Québec G1J 2G3, Canada. E-mail: andre.parent@anm.ulaval.ca

Received 21 August 2002; Revised 21 November 2002; Accepted 23 December 2002

DOI 10.1002/cne.10627

Published online the week of April 14, 2003 in Wiley InterScience (www.interscience.wiley.com).

putamen located beneath the anterior limb of the internal capsule, the Acb forms the part of the VST that roughly corresponds to the fundus striati of Brockhaus, who included the bed nucleus of the stria terminalis (BST) in this entity (Brockhaus, 1942). In current usage, however, the term *fundus striati*, as applied to primates, does not include the BST. In humans, numerous compact clusters of small neurons occur at the point of convergence between the Acb and adjacent basal forebrain structures, such as the claustrum and the diagonal band of Broca (DB). These islands, named *interface islands* by Heimer et al. (1999), are prominent features of the extended amygdala. They form a topographic border that is thought never to be transgressed by the extension of the Acb.

As is the case for the dorsal striatum, the compartmental organization of the VST has attracted much attention. For example, the Acb in rodents has been divided into three distinct territories (core, shell, and rostral pole) based on differences in chemical composition (Zaborszky et al., 1985; Voorn et al., 1989; Groenewegen et al., 1991; Jongen-Relo et al., 1993; Meredith et al., 1993; Koob et al., 1993) and fiber connections (Heimer et al., 1991; Zahm and Brog, 1992; Brog et al., 1993; Zahm and Heimer, 1993). The core of the Acb consists of small and densely packed cells; it expresses intense calbindin D-28k (CB) immunoreactivity but weak substance P (SP) immunostaining. The shell of Acb is composed of large and loosely arranged cells; it is mostly devoid of CB but expresses high SP immunoreactivity (Voorn et al., 1989; Meredith et al., 1989; Groenewegen et al., 1991; Zahm and Brog, 1992). A difference between the core and the shell of the rodent Acb was also noted with respect to the somatodendritic morphology of projection neurons (Meredith et al., 1992).

The core and shell dichotomy has also been applied to the primate Acb (Voorn et al., 1994, 1996; Ikemoto et al., 1995). In primates, however, the core region appears contiguous with the rest of the striatum, from which it cannot be easily distinguished. In contrast, the shell has several histochemical and hodological features that make it different from the rest of the striatum. For example, in all species examined, the core region of the Acb differs from the rest of the VST by its relatively low levels of CB immunoreactivity (Zahm and Brog, 1992; Zahm and Heimer, 1993; Jongen-Relo et al., 1994; Meredith et al., 1996).

In humans, evidence for a subdivision of the Acb into core and shell regions was obtained following studies of the distribution of opiate and dopamine receptors (Voorn et al., 1994, 1996; Vonkeman et al., 1996). In comparison with the core, the shell subdivision of the human Acb was markedly enriched in kappa opiate and dopamine D1 and D3 receptors, as well as in acetylcholinesterase (AChE). The human Acb was also subdivided into lateral and medial sectors on the basis of differences in CB and calretinin (CR) immunoreactivity (Morel et al., 2002).

In the present study, we applied immunohistochemical and histochemical procedures to postmortem human brain material obtained from healthy individuals to study the neurochemical organization of the VST. We analyzed the distribution of CB, limbic system-associated membrane protein (LAMP), SP, CR, choline acetyltransferase (ChAT), and AChE in the various sectors of the human VST. Special attention was paid to the chemical properties of the core and shell divisions of the Acb as well as to other basal forebrain structures that surround the VST, such as the interface islands, the claustrum (Cl), the DB, and the BST.

TABLE 1. Clinical Data on the Human Cases Used in This Study

Case	Sex	Age (years)	Postmortem delay (hours)	Cause of death
H-1	Female	71	5	Myocardial infarction
H-2	Male	70	10	Cardiac arrest
H-3	Female	76	4	Head injuries
H-4	Female	38	18	Drug overdose
H-5	Male	45	12	Myocardial infarction
H-6	Male	68	12	Pulmonary embolism

Abbreviations

AC	anterior commissure
Acb	nucleus accumbens
AChE	acetylcholinesterase
BST	bed nucleus of stria terminalis
BSTL	lateral division of BST
BV	blood vessel
CB	calbindin D-28K
Cd	caudate nucleus
ChAT	choline acetyltransferase
Cl	claustrum
CR	calretinin
Cr	core region of Acb
DB	diagonal band of Broca
ec	external capsule
ex	extreme capsule
GPe	external segment of globus pallidus
IC	internal capsule
Ii	interface islands
LAMP	limbic system associated membrane protein
NUDAP	neurochemically unique domains in the Acb and putamen
Put	putamen
S	shell region of the nucleus accumbens
SI	substantia innominata
SP	substance P
Sr	shell division of Acb
VCl	ventral portion of claustrum
VDB	vertical limb of DB
VP	ventral pallidum
VST	ventral striatum

MATERIALS AND METHODS

Subjects

The present observations are based on analysis of post mortem material obtained from six healthy individuals, with no clinical or pathological evidence of neurological or psychiatric disorders (Table 1). The material was kindly provided by Dr. Michel Marois, Service de Pathologie, Hôpital Saint-François d'Assise, Québec, and our protocol was approved by the Laval University Committee on Ethics in Research. The brains were sliced fresh into 0.5-cm-thick slabs that were fixed by immersion in 4% paraformaldehyde at 4°C for 4–5 days. After fixation, the slabs were immersed in 15% sucrose in 0.1 M phosphate-buffered saline (PBS; pH 7.4) at 4°C until they sank. They were then stored in PBS with 15% sucrose and 0.1% sodium azide in a refrigerator.

The slabs containing the VST were cut with a freezing microtome into 50-μm-thick coronal sections that were serially collected in cold PBS. Series of adjacent sections were then processed either immunohistochemically for the visualization of CB, CR, LAMP, SP, and ChAT or histochemically for AChE. The immunohistochemical protocol

TABLE 2. Information on the Antibodies Used in This Study[1]

Antibody	Source	Animal source	Dilution	Incubation	Revelation
CB	Sigma	Mouse (mAb)	1:2,500	Overnight/4°C	DAB
LAMP	P. Levitt	Mouse (mAb)	1:2,500	48 Hours/4°C	DAB
CR	Swant	Rabbit (pAb)	1:2,500	Overnight/4°C	DAB
ChAT	Chemicon	Goat (pAb)	1:100	72 Hours/4°C	DAB
SP	Medicorp	Rat (mAb)	1:50	Overnight/4°C	DAB

[1]CB, calbindin; LAMP, limbic system-associated membrane protein; CR, calretinin; ChAT, choline acetyltransferase; SP, substance P; DAB, 3,3′-diaminobenzidine tetrahydrochloride. mAb, monoclonal antibody; pAb, polyclonal antibody.

used to visualize CB, CR, SP, and ChAT was described in detail elsewhere (Prensa et al., 1999). In brief, after three rinses of 10 minutes each in PBS, the free-floating sections were placed for 30 minutes at room temperature in a solution composed of 10% hydrogen peroxide (H_2O_2; 3%) plus 90% ethanol (50%) to eliminate endogenous peroxidase activity. Sections were then incubated in a solution containing the primary antibody, 0.1% Triton X-100, and 2% normal horse serum (for CB), normal goat serum (for CR), or normal rabbit serum (for SP and ChAT). Incubation conditions and sources of primary antisera are specified in Table 2. The CB antibody was a highly specific mouse monoclonal antibody (clone 300; Celio, 1990). The polyclonal anti-CR antibody was produced in rabbit by immunization with recombinant human CR; it did not cross-react with CB or other known calcium-binding proteins (Schwaller et al., 1993). The SP antibody was a rat monoclonal antibody that did not cross-react with other known mammalian brain peptides (Cuello et al., 1979), whereas the anti-ChAT was an affinity-purified polyclonal antibody raised against goat ChAT (Chemicon, Temecula, CA; Grosman et al., 1995).

After three rinses of 10 minutes each in PBS, the sections were incubated for 1 hour at room temperature in the secondary antibodies, which were biotinylated horse IgG (for CB), biotinylated goat IgG (for CR), and biotinylated rabbit IgG (for SP and ChAT). After three more rinses in PBS, the sections were reincubated for 1 hour at room temperature in 2% avidin-biotin complex (ABC; Vector, Burlingame, CA) and then washed twice in PBS and once in 0.05 M Tris buffer (pH 7.6). The bound peroxidase was revealed by placing the sections in a medium containing 0.05% 3,3′-diaminobenzidine tetrahydrochloride (DAB; Sigma, St. Louis, MO) and 0.0018% H_2O_2 (30%) in 0.05 M Tris buffer (pH 7.6) at room temperature. The reaction was stopped after about 5 minutes by washing once in 0.05 M Tris buffer (pH 7.6) and twice in PBS.

The immunohistochemical protocol used to reveal LAMP was similar to the one described above except that the amount of Triton X-100 was reduced to 0.005% in the incubation medium containing the primary antibody and to 0.025% in the solution containing the secondary antibody. The LAMP monoclonal antibody (clone 2G9) was kindly donated by Dr. Pat Levitt, John F. Kennedy Center, Vanderbilt University, and its method of production and specificity have been reported in detail elsewhere (Levitt, 1984; Zacco et al., 1990).

All immunohistochemical sections were mounted on gelatin-coated slides that were air dried, rinsed in distilled water, and dehydrated through passages in ascending grades of alcohol. Sections were cleared in toluene and coverslipped with Permount. Some sections were treated as described above except that the primary antibody was omitted from the incubation medium. These sections remained virtually free of immunostaining and served as controls.

AChE histochemistry

A modification of the Geneser-Jensen and Blackstad's procedure (1971) was used to visualize AChE (see Prensa et al., 1999). Briefly, the sections were washed in distilled water and incubated during a period that ranged from 3 to 6 hours in a solution composed of distilled water to which were added sequentially ethopropazine (0.023%), acetylthiocholine iodide (0.1%), glycine (0.075%), cupric sulfate (0.050%), and anhydrous sodium acetate (0.410%). The final pH of the solution was adjusted to 5 by the addition of some drops of glacial acetic acid. The precipitate was visualized by placing the sections for 2–3 minutes in a distilled water solution containing 10% potassium ferricianyde. The reaction was stopped by extensive rinsing in distilled water, and the sections were mounted, dehydrated, cleared, and coverslipped as described above. Control sections were processed similarly, except that acetylthiocholine iodide was omitted from the incubation medium.

Data analysis

The VST was examined at six equally spaced levels that covered the entire rostrocaudal extent of the VST (Fig. 1). The first level was slightly rostral to the plane named *Kl-B1* in the photographic atlas of the human basal forebrain of Heimer et al. (Sakamoto et al., 1999; Heimer et al., 1999), whereas levels 2, 3, 4, 5, and 6 corresponded, respectively, to planes Kl-B2, Kl-B3, Kl-B4, Kl-B5, and Kl-B6 of the same atlas. This atlas was also used to identify the various basal forebrain structures that surrounded the VST at each of these six anteroposterior levels (Fig. 1).

Series of six adjacent sections through the VST of all brains, taken at each of the six chosen levels, were stained for the markers of interest to allow a direct comparison of the distribution of each marker over a 50–100-μm distance. Direct "negative" prints were taken of all the sections to visualize the overall distribution of the various chemical markers in the VST. The negative print images were obtained by directly printing immunostained sections inserted in a photographic enlarger (Focomat V35; Leitz). Furthermore, the contours of sections and the boundaries between the various chemospecific regions on each section were drawn with the help of a microscope equipped with a camera lucida in three of the six cases examined in the present study. These drawings were made on transparent paper sheets that were superimposed to delineate regions of correspondence and mismatch in the distribution of the markers. The results obtained from these three brains are summarized schematically in Figure 1. These three particular cases (H-2, H-4, and H-6; see Table 1) were chosen because their sets of sections were covering the entire rostrocaudal extent of the VST and included all of the surrounding structures of interest. Despite some slight variations in the overall intensity of the labeling, no significant differences were noted in the comparative pattern of distribution of the different chemical markers in the six brains examined in this study, irrespective of age, sex, and post mortem delay.

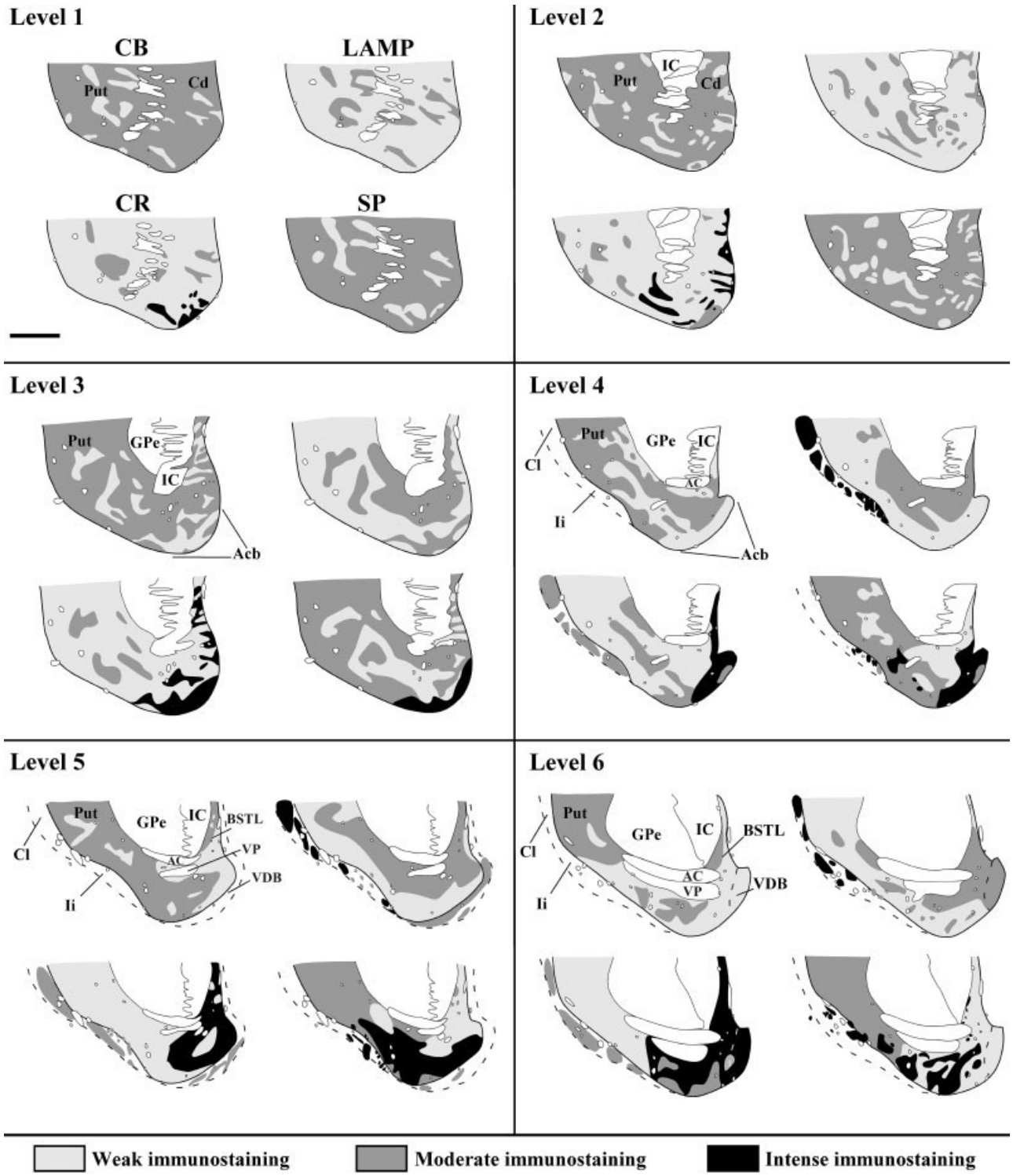

Fig. 1. Schematic drawings depicting the distribution of immunostaining for CB, LAMP, CR, and SP in the VST and some adjacent basal forebrain structures in human. The drawings represent equally spaced sections taken at six different rostrocaudal levels, level 1 being the most rostral and level 6 the most caudal. Different shades of gray are used to indicate the intensity of the staining of the neuropil for each chemical marker (see caption at bottom). Scale bar = 5 mm.

The exact distribution of the CR-immunoreactive (-ir) and ChAT-ir neurons with respect to the core/shell territories of the Acb was plotted with the camera lucida. Additionally, photomicrographs were taken at different magnifications to illustrate in more detail the patterns of distribution of the various types of immunostaining as

well as the morphological features of some chemospecific neurons. The images were digitally captured (AGFA Studiocam, Woburn, NA) and handled with Adobe Photoshop (version 5.5; Adobe, San Jose, CA). The final rendering of the drawings was made by using Canvas software (version 6.0; Deneba Systems, Inc., Miami, FL). Estimates of the smaller and larger diameters of the perikarya of the various types of immunoreactive neurons were obtained by using an eyepiece graticule at ×40. These measurements were made only on labeled neurons that had an intact perikaryal contour and clear nuclear profile.

RESULTS

General patterns of immunostaining in the VST

CB. In CB-immunostained sections, a multitude of CB-ir perikarya was scattered in a moderately stained neuropil. Furthermore, conspicuous CB-poor regions were unevenly distributed throughout the rostrocaudal extent of the VST (Figs. 1, 2A,E, 3A, 4A, 8A, 11D). The weak staining of the CB-poor areas reflected a lightly stained neuropil and a paucity of CB-ir perikarya at these levels (Figs. 2E, 4A, 11D). The size and shape of the CB-poor zones varied markedly along the rostrocaudal extent of the VST: They were small with diffuse edges rostroventrally, elongated along the mediolateral axis in the Acb, and strikingly large caudally (Figs. 1, 2E, 4A). Some fiber fascicles that detached from the internal capsule and spread out in the rostroventral sector of the caudate nucleus and putamen and in the Acb were darkly stained for CB. These CB-ir fibers were more abundant in the putamen than in the caudate nucleus and also occurred within the CB-poor patches of the VST. The CB-ir neurons in the VST were of medium size and strikingly resembled the medium-sized spiny projection neurons that populated the dorsal striatum. No large CB-ir neurons were observed in the VST, despite the fact that many such neurons were encountered in the lateral portion of the dorsal two-thirds of the putamen at the same anteroposterior levels.

LAMP. LAMP was heterogeneously scattered throughout the rostrocaudal extent of the VST (Fig. 1). At rostral levels, LAMP was distributed according to a mosaic-like pattern that was particularly obvious in the ventral portion of the caudate nucleus and putamen (Figs. 1, 2B). At more caudal levels, however, LAMP immunostaining was more uniform and was largely confined to the striatal sector that surrounds the anterior commissure and the ventral aspect of the external segment of the globus pallidus (GPe) and internal capsule (Figs. 1, 3B, 8B). At the most caudal level, LAMP remained confined to the ventromedial aspect of the VST and to several small areas scattered beneath the ventral pallidum (Figs. 1, 11C). Microscopically, LAMP immunostaining appeared as a multitude of small punctate structures scattered within a dense neuropil (Fig. 11C).

CR. The VST contained numerous aspiny CR-ir cell bodies scattered within a dense and heterogeneously distributed neuropil (Figs. 1, 2C,F,I, 3C, 4B, 8C). Rostrally, small patches of moderate or intense CR-ir neuropil were scattered in the ventral region of the caudate nucleus and putamen (Figs. 1, 2C,F,I). More caudally, however, the CR-ir neuropil was very intense, more uniformly distributed, and largely confined to the medial part of the VST (Figs. 1, 3C, 4B, 8C, 10B). In contrast to the neuropil, CR-ir cell bodies abounded particularly in the lateral part of the VST (Fig. 5B). These neurons belonged to two types: 1) medium-sized neurons with round or fusiform perikarya of 10–25 μm in diameter that emitted two to four primary aspiny dendrites (Table 3, Figs. 2I, 5F–H) and 2) large neurons with a round or fusiform cell body that ranged from 26 to 40 μm in diameter and from which emerged three or four primary aspiny dendrites (Table 3, Figs. 2I, 5F).

SP. The immunostaining for SP in the VST was heterogeneous and followed a dorsoventral increasing gradient, which was especially noticeable medially (Figs. 1, 2D, 3D, 8D). This heterogeneity stemmed principally from the intermingling of SP-poor and SP-rich areas scattered along the entire rostrocaudal extent of the VST (Figs. 1, 2D,G, 3D, 4C, 6A, 8D, 11A,B). Rostrally, the SP-poor zones were small, unevenly distributed, and better defined in the caudate nucleus than in putamen (Figs. 1, 2D,G). At midlevels, the SP-poor zones were larger and mainly confined to the ventromedial aspect of the VST (Figs. 1, 3D, 4C, 6A). Caudally, numerous intensely stained SP-ir tubular profiles, most probably pallidal dendrites covered with striatofugal SP-ir terminals, occurred in the VST. At the most caudal level, the SP immunostaining was patchy, indistinctly delineated, and appeared to be composed of a mixture of striatal and pallidal tissue (Fig. 11A,B).

ChAT and AChE. The human VST displayed intense staining for the cholinergic markers used in this study. The VST was pervaded by a rich array of neurons, fibers, and terminals or terminal-like structures, all displaying ChAT immunoreactivity (Figs. 2H, 4D, 5C,D, 9D, 11E). The ChAT-ir perikarya were round, polygonal, or fusiform, with a maximum diameter that ranged from 25 to 45 μm (Table 3, Fig. 5C,D). Regional variations in the intensity of the AChE and ChAT neuropil resulted in a mosaic-like pattern of lightly stained zones embedded in a more densely stained background (Figs. 2H, 4D, 11E). In ChAT- and AChE-stained sections, the regions of weak staining were generally less well defined and more complex in shapes than in other stained sections. Furthermore, the boundaries of the ChAT- and AChE-poor zones were usually less well defined in the putamen than in the caudate nucleus.

Comparisons of the various patterns of immunostaining in the VST

Rostral VST. At levels 1 and 2, all markers present in the ventral portion of the caudate nucleus and putamen were distributed according to a mosaic-like pattern (Figs. 1, 2A–D). As is the case for the dorsal striatum, the CB-poor zones in the VST were in register with LAMP-ir patches, which were largely devoid of SP, ChAT, and AChE (Fig. 2A–G). The intensity of LAMP immunostaining was approximately the same in all patches, except for some slightly more intense patches located ventromedially in the caudate nucleus. Some of the CB-poor zones of the VST displayed a more CR-ir neuropil than the surrounding tissue (Figs. 1, 2C,F,I). The patches that showed a highest density of CR-ir neuropil were mainly confined to the ventromedial aspect of the caudate nucleus and putamen, and in some cases they did not match CB-poor regions (Fig. 1). These ventrally located patches harbored some medium-sized CR-ir neurons, with two or three short aspiny dendrites, but were devoid of the typical large

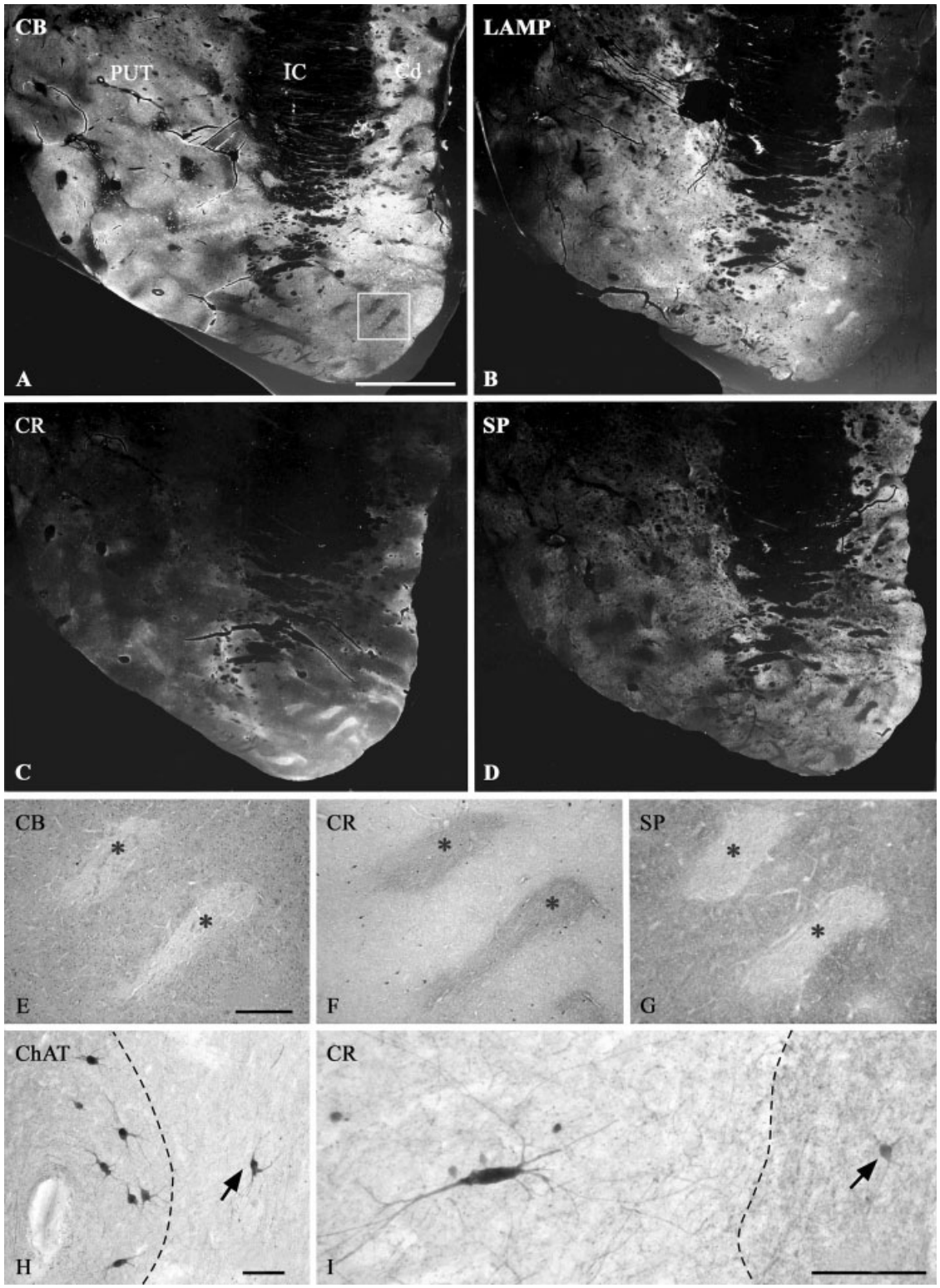

Fig. 2. **A–D:** Direct prints showing the immunostaining for CB, LAMP, CR, and SP in the rostral part (level 2) of the VST, as seen in four adjacent sections. **E–G:** Photomicrographs showing two typical patches in the VST (see box in A), as seen in adjacent sections immunostained for CB, CR, and SP. **H:** High-power view of some ChAT-ir neurons located close to, as well as within (arrow), a patch in the VST. The dashed line delimits the patch. **I:** High-power view of a large CR-ir neuron lying near a patch located in the ventral part of the the head of the caudate nucleus. A smaller CR-ir neuron (arrow) also occurs within the patch, which is delimited by the dashed line. Scale bar = 5 mm in A, 250 μm in E, 100 μm in H, I.

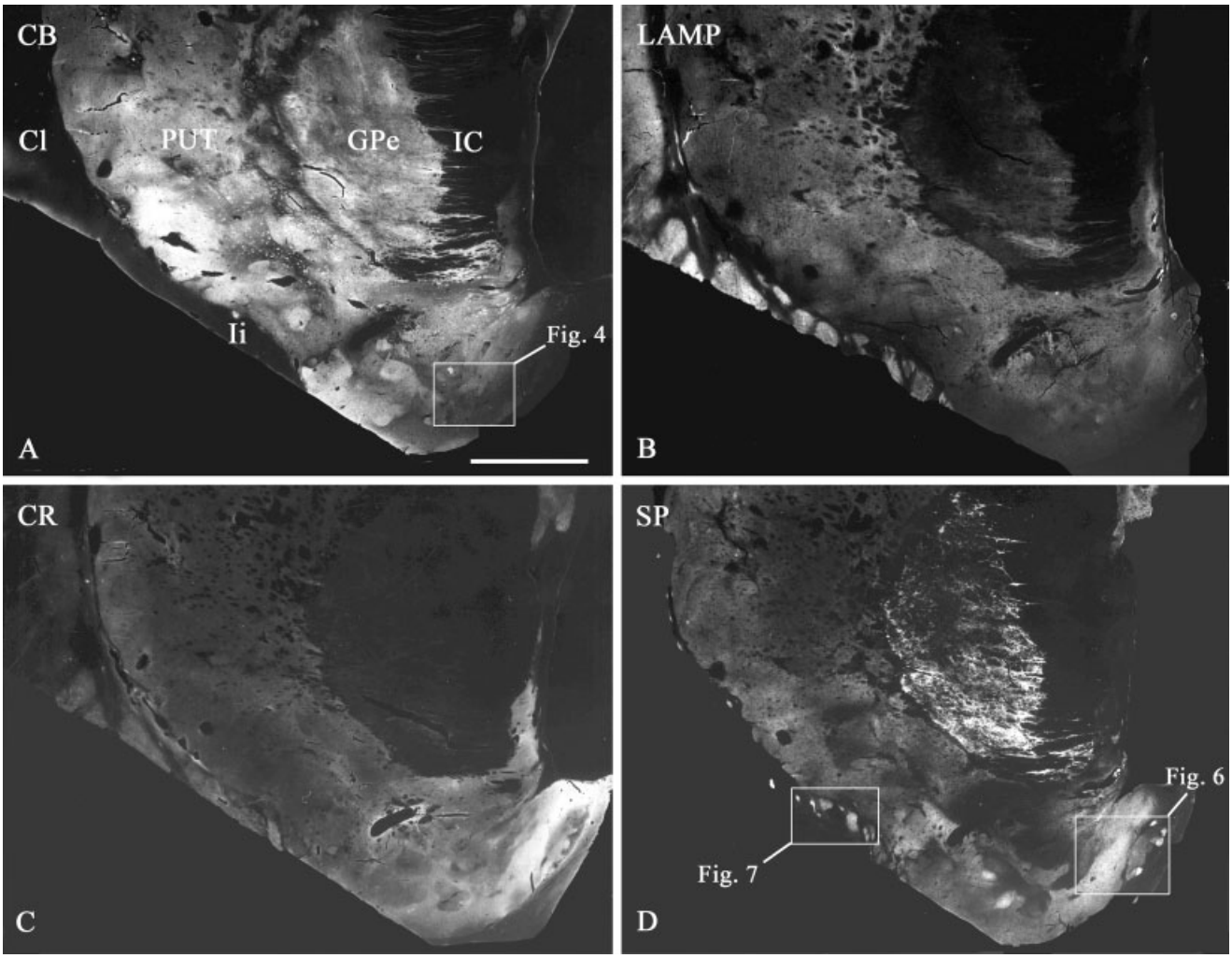

Fig. 3. Direct prints showing immunostaining for CB, LAMP, CR, and SP in the VST (level 4), as seen in four adjacent sections. The boxes in A and D delimit the areas shown in the corresponding figures. Scale bar = 5 mm.

CR-ir neurons (Fig. 2I). Some cholinergic neurons were also encountered within the CR-ir patches, but they were less numerous than in the surrounding tissue (Fig. 2H).

Shell and core divisions of Acb. At level 3, a CB-poor region occurred within the most ventral aspect of the VST. This region stands out by its moderate LAMP immunostaining and dense CR- and SP-ir neuropil (Fig. 1, Table 4), but it was not easily distinguishable from the adjacent tissue in sections immunostained for AChE and ChAT. By virtue of its CB-poor and SP-rich nature, this region appears to correspond to the shell division of the Acb. More caudally, this accumbal region expanded dorsomedially to reach the ventral tip of the lateral ventricle at level 4. The shell division of the Acb at this level is bordered by several cellular islands, including the insula magna (Figs. 1, 3D, 6). The core region of the Acb was more darkly stained for CB and LAMP than the shell but was notably less immunoreactive for CR and SP (Figs. 1, 3, 4A–C, 6A,C, Table 4). No clear boundary between the shell and core could be established in sections stained for AChE and ChAT (Figs. 4D, 6B), and none of the chemical markers used here provided a clear dorsal limit between the core and the dorsal striatum (Fig. 3). Numerous CB-poor strips were oriented mediolaterally between the medial edge of the striatum and the medial boundary of the internal capsule at the level 3 (Fig. 1). These CB-poor strips were also enriched in CR but largely devoid of SP, ChAT, and AChE (Fig. 1). The medial aspect of the shell showed a very intense CR-ir neuropil but harbored very few CR-ir neurons, whereas the inverse occurred more laterally (Figs. 1, 3C, 5B). The shell also displayed a mediolaterally increasing gradient of CB immunostaining, and the staining intensity for ChAT and AChE was slightly weaker in the medial aspect of the shell than in the core (Fig. 6B), whereas the inverse was true at more lateral levels (Fig. 4D, Table 4).

Numerous ChAT- and CR-ir cell bodies were encountered in the Acb, and there was some variation between the core and the shell with respect to the size and morphological characteristics of these chemospecific neurons

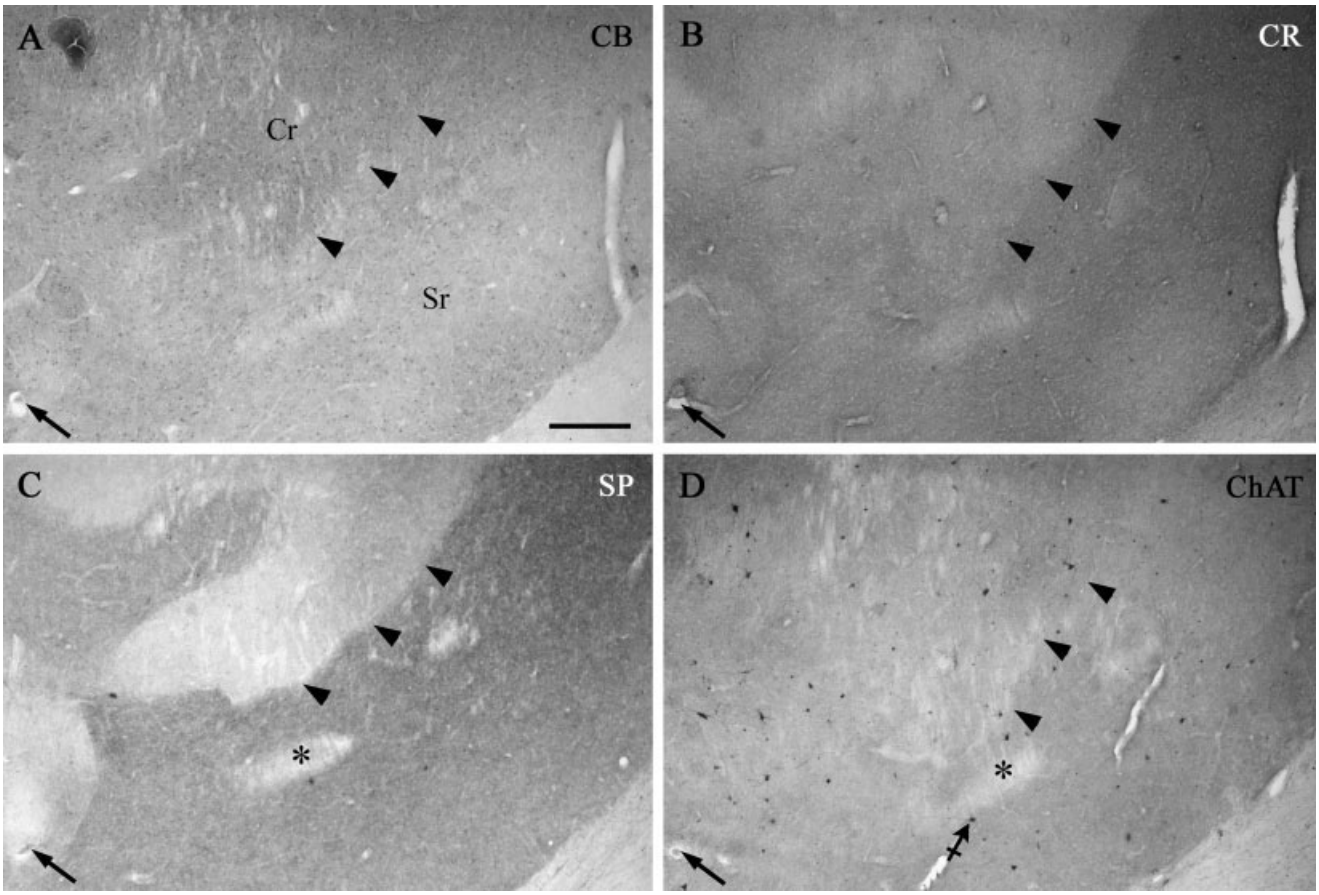

Fig. 4. **A–D:** Photomicrographs showing immunostaining for CB, CR, SP, and ChAT expressed by the core (Cr) and the shell (Sr) divisions of the nucleus accumbens. The exact location of the area illustrated is shown in Figure 3A. Arrowheads indicate the limit between the core and the shell, and arrows point to a blood vessel that serves as a landmark. Asterisks indicate a sector of the core that is embedded within the shell. The crossed arrow in D points to a ChAT-ir neuron in the shell. This neuron is shown at a higher magnification in Figure 5E. Scale bar = 400 μm.

(Table 3). In the shell, the ChAT-ir perikarya were round or polygonal, had a maximal diameter that ranged between 25 and 35 μm, and emitted two to four long and poorly branched aspiny primary dendrites (Fig. 5D). In the core, the ChAT-ir perikarya were round, polygonal, or fusiform; had a maximal diameter that ranged between 25 and 45 μm; and gave rise to three to six highly branched dendrites (Fig. 5C). Overall, the ChAT-ir neurons encountered at the medial aspect of both the shell and the core were slighter smaller and less branched than those located more laterally in each Acb subdivisions (Table 3). The ChAT-ir cell bodies located in the most lateral sector of the core had a large (maximal diameter of 30–45 μm), round or polygonal perikaryon from which emerged four to seven short aspiny dendrites that branched frequently. These cholinergic neurons resembled those located in the adjoining dorsal striatum (Table 3).

The Acb was also populated by large and medium-sized CR-ir neurons. In the core of the Acb, the large (maximal diameter 26–40 μm) CR-ir neurons had a round, polygonal, or fusiform perikaryon that gave rise to three or four aspiny and highly branched dendrites (Table 3, Fig. 5F). The core also contained medium-sized (maximal diameter 10–25 μm) CR-ir neurons, whose round or fusiform perikaryon gave rise to two to four smooth, poorly ramified primary dendrites (Fig. 5F). At the shell level, the large (maximal diameter 26–35 μm) CR-ir neurons occurred only in the lateral half of this Acb component. These neurons possessed a round or polygonal cell body that gave rise to three or four highly ramified dendrites. In contrast, the medium-sized (maximal diameter 15–25 μm) CR-ir neurons were present along the mediolateral extension of the shell. These neurons had round or fusiform cell bodies that gave rise to two to four poorly ramified primary dendrites (Table 3, Fig. 5G,H). As is the case for the ChAT-ir neurons, the CR-ir neurons tended to be smaller in the medial aspect of the Acb than in its lateral sector (Table 3).

The ChAT-ir neurons were rather uniformly distributed in the ventral one-third of the putamen and Acb, whereas the density of the CR-ir neurons in the ventral one-third of the putamen was notably higher than that in the Acb (Fig. 5A,B). Except for the medial aspect of the shell, which harbored only a few CR-ir neurons (Fig. 5B), no significant differences were noted between the core and the shell divisions of Acb with respect to the distribution of CR- and ChAT-ir neurons. Some ChAT-ir neurons had processes that crossed the boundary between the shell and the core

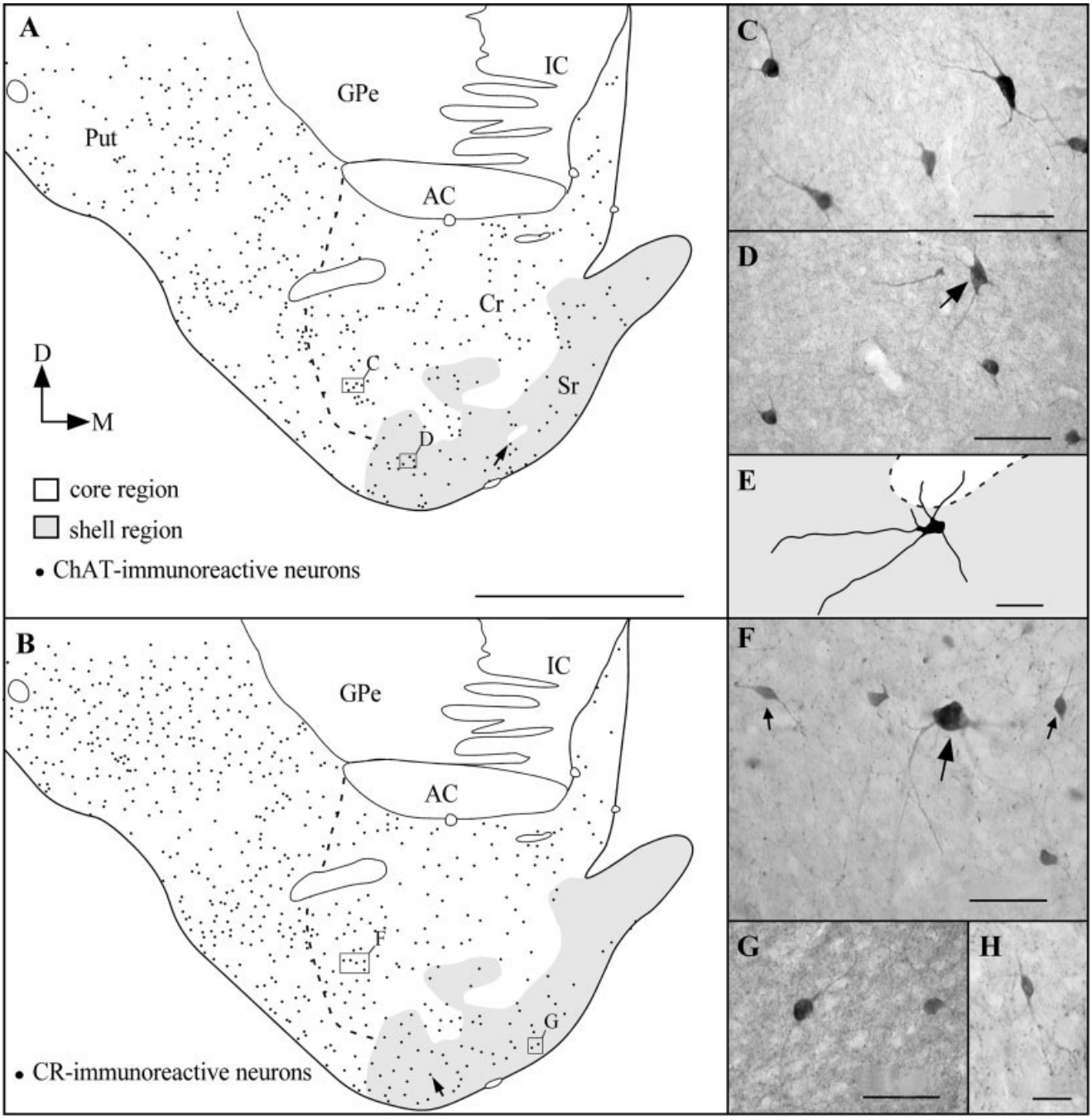

Fig. 5. **A,B:** Camera lucida drawings illustrating the distribution of ChAT- and CR-ir neurons with respect to the shell (Sr) and core (Cr) regions of the nucleus accumbens and the ventral putamen. The plane of section corresponds to level 4 (see Fig. 1). Each dot represents one neuron. The boundaries between the shell and the core and the core and the ventral one-third of the putamen were established with SP immunostaining. The fuzzy transition between the core of the accumbens and the ventral putamen is indicated by a dashed line. Boxes mark the location of the neurons illustrated in the corresponding photomicrographs, and arrows in A and B point to the neurons that are illustrated at a higher magnification in E and H, respectively. **C,D:** Photomicrographs showing some ChAT-ir neurons in the core (C) and one multipolar neuron (arrow) and two smaller cholinergic cells lying in the shell (D) of the nucleus accumbens. **E:** Camera lucida drawing of the somatodendritic domain of a ChAT-ir neuron located in the shell (see arrow in A). Note that this neuron, which is also indicated by the crossed arrow in Figure 4D, is located close to a small sector of the core embedded within the shell (see asterisk in Fig. 4D). **F:** Example of one large (large arrow) and several medium-sized (small arrows) CR-ir neurons in the core. **G,H:** Examples of three CR-ir neurons located at different mediolateral levels in the shell. The neuron illustrated in H corresponds to the one indicated by the arrow in B. Scale bar = 5 mm in A, in C–G = 100 μm, in H = 50 μm.

TABLE 3. Morphological Features of Cholinergic (ChAT-ir) and Calretinin-ir Neurons in Nucleus Accumbens and Dorsal Striatum, and Minimum and Maximum Diameters of Each Neuronal Type in Each Accumbal Region

	Nucleus accumbens				
	Core		Shell		Dorsal striatum
ChAT-ir neurons					
Perikarya	Round/polygonal/fusiform (25–45 μm)		Round/polygonal (25–35 μm)		Round/polygonal (30–45 μm)
	Medial half 25–35 μm	Lateral half 25–45 μm	Medial half 25–30 μm	Lateral half 25–35 μm	
Primary dendrites	3–6 Frequently ramified		2–4 Poorly ramified		4–7 Frequently ramified
CR-ir neurons, large					
Perikarya	Round/polygonal/fusiform (26–40 μm)		Round/polygonal (26–35 μm)		Round/triangular (26–45 μm)
	Medial half 26–35 μm	Lateral half 26–40 μm	Medial half Not found	Lateral half 26–35 μm	
Primary dendrites	3–4 Frequently ramified		3–4 Frequently ramified		4–7 Frequently ramified
CR-ir neurons, medium-sized					
Perikarya	Round/fusiform (10–25 μm)		Round/fusiform (15–25 μm)		Round/triangular (10–25 μm)
	Medial half 10–25 μm	Lateral half 15–25 μm	Medial half 15–25 μm	Lateral half 15–25 μm	
Primary dendrites	2–4 Poorly ramified		2–4 Poorly ramified		2–3 Poorly ramified

(Fig. 5E), whereas others occurred along the ventral boundaries of the VST, most probably corresponding to displaced cells of the nucleus of the diagonal band.

Caudal VST. The distribution pattern of the chemical markers was significantly more complex at levels 5 and 6 than at more rostral levels (Fig. 1). The core and shell division of the Acb was no longer discernible, and the chemical profile of the VST consisted of numerous small immunoreactive areas separated by unstained zones that intermingle with substantia innominata regions, including the nucleus basalis of Meynert (Fig. 11). Laterally, the VST was clearly delineated from the putamen, whereas medially it merged imperceptibly with the lateral part of the bed nucleus of the stria terminalis (BSTL) and the vertical limb of the DB (VDB; Figs. 1, 8, 9).

At these caudal levels, the VST was intensely stained for CR (Figs. 1, 8C, 10B) but poorly labeled for CB, except for small areas clustered below the ventral pallidum that displayed a moderate CB immunostaining (Figs. 1, 11D). LAMP was confined to the striatal region that lay beneath the ventral pallidum and internal capsule at level 5 (Figs. 1, 8B), whereas it prevailed within the medial sector of the VST and in small areas scattered more ventrolaterally at level 6 (Figs. 1, 11C). The SP staining was confined to a large, mediolaterally oriented zone at level 5 (Figs. 1, 8D), whereas it broke out into numerous small SP-ir areas separated by irregular cell-poor streaks at level 6 (Figs. 1, 11A,B). The staining for cholinergic markers included both poorly and intensely stained zones that were distributed according to a mediolaterally increasing gradient (Fig. 11E). There were zones in which the AChE staining was considerably more intense than the ChAT immunoreactivity.

Basal forebrain structures adjacent to VST

Interface islands. At level 4, the shell of the Acb was bordered medially and ventrally by island-like cell clusters composed of closely packed neurons of various sizes. These cell islands, which are often referred to as *interface islands* (Heimer, 2000), showed patterns of immunostaining that contrasted with the pattern of the VST (Figs. 3D, 6). Other similar islands located alongside the ventral putamen, at its border with the external capsule, were observed from level 4 to level 6 (Figs. 1, 3D, 7). Two types of islands occurred beneath the shell of the Acb: small islands markedly enriched in SP, AChE, and ChAT but largely devoid of CR that surrounded a larger island exhibiting a pattern of staining opposite to that of the small islands (Figs. 3D, 6). These islands showed a weak immunostaining for CB and LAMP similar to that of the shell (Figs. 1, 3A,B). Some ChAT-ir neurons were located at the interface between the shell and these islands, and their dendrites entered both structures (Fig. 6D). Other ChAT-ir cells occurred at the boundaries between the small and the larger islands beneath the shell. An intense LAMP immunostaining characterized the islands that lay along the ventral putamen, at its border with the external capsule (Figs. 1, 3B, 7B). Some of these islands also displayed a high level of SP and AChE staining (Figs. 1, 3D, 7C,D). Some ChAT- and CR-ir neurons were also scattered among the numerous fibers and terminals-like structures that occurred in these islands (Fig. 7E,F). These neurons did not differ morphologically from the ChAT- and CR-ir neurons located in the putamen. A small cluster of large ChAT-ir neurons, together with a few voluminous CR-ir neurons embedded within a dense spot of CR-ir neuropil, occurred at the junction between the ventral putamen and the external capsule (Fig. 7G,H). Based on its location, this cluster of magnocellular neurons might correspond to one of the laterally placed clusters of the basal nucleus of Meynert.

Claustrum. The more dorsally located interface islands, which lay alongside the lateral edge of the putamen, were separated from the claustrum (Cl) by the external capsule. However, the ventral portion of the claustrum (VCl) widened in the temporal lobe and abutted the more ventrally located islands and the lateral edge of the VST (Fig. 10A). The Cl and VCl displayed an intense and uniform punctate-like LAMP staining (Figs. 1, 3B, 8B, 10A,C) but were largely devoid of CB, SP, ChAT, and AChE (Figs. 1, 3A,D, 8A,D). Numerous CR-ir neurons were scattered within moderately stained CR-ir neuropil throughout the Cl and VCl (Figs. 1, 10B,D,E). Most CR-ir cells were bipolar, with round to elongated cell bodies (maximal diameter 10–15 μm) and beaded dendrites (Fig. 10D,E). Occasionally, some of these CR-ir cells formed

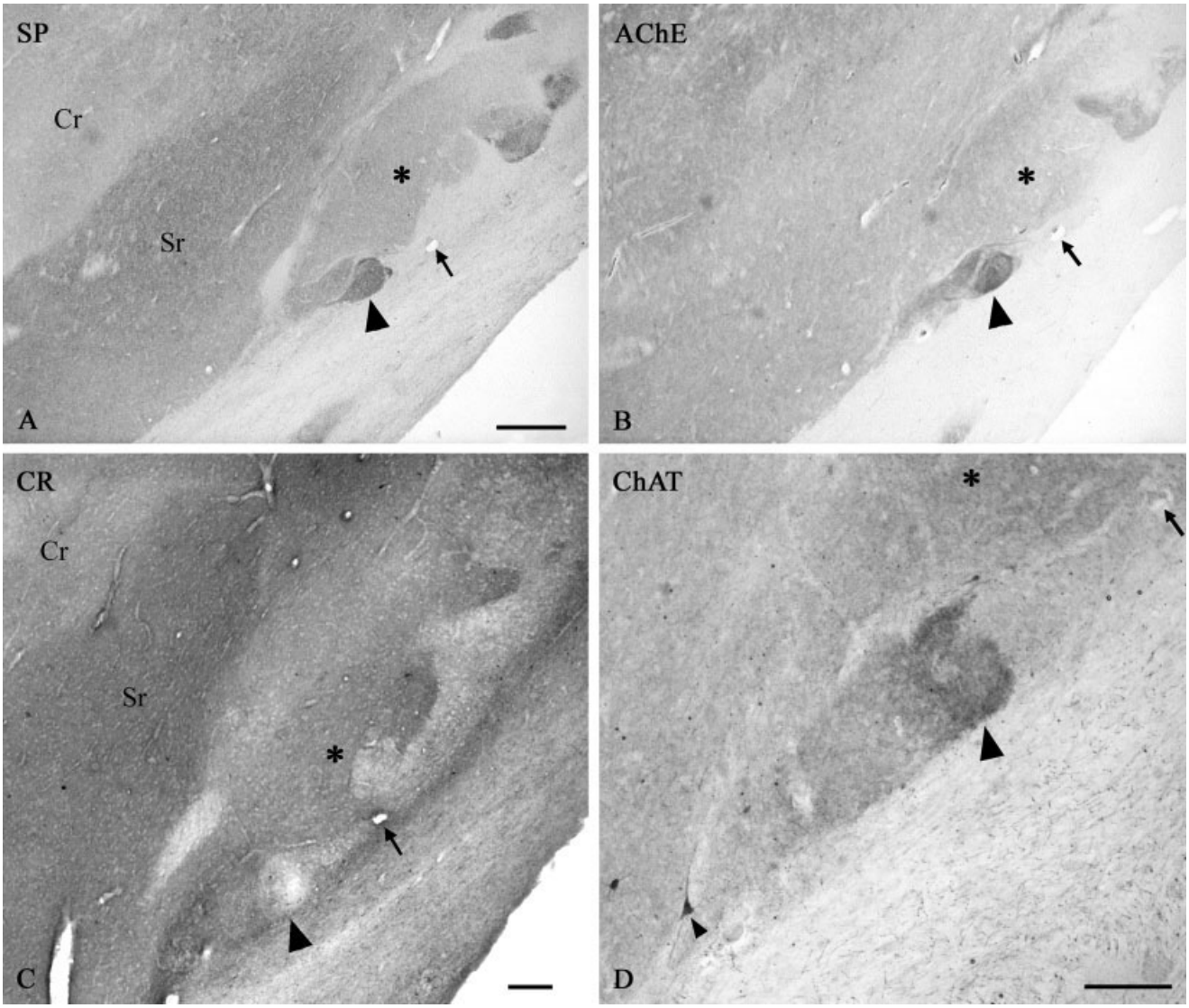

Fig. 6. Photomicrographs of interface islands lying along the medial aspect of the shell of the nucleus accumbens, as seen in adjacent sections immunostained for SP, AChE, CR, and ChAT. The exact location of this field is indicated in Figure 3D. Arrows point to a blood vessel that serves as a landmark, and the core (Cr) and shell (Sr) regions of nucleus accumbens are labeled in A and C. Note several small islands, one of which is indicated by large arrowheads, that are intensely stained for SP, AChE, and ChAT but devoid of CR. These small islands surround a larger island (asterisk), which displays an opposite pattern of immunostaining. The small arrowhead in D points to one ChAT-ir neuron located at the interface between the shell and one of the small islands. Scale bar = 500 μm in A (applies to B), in C,D = 200 μm.

densely packed clusters (Fig. 10E). Larger CR-ir neurons (maximal diameter 20–30 μm) displaying three or four primary dendrites were also observed in the Cl and VCl. Many of these large neurons were located at the medial or lateral margins of this structure with dendrites invading the external or extreme capsules. The Cl and the VCl also harbored some lightly stained, small multipolar CB-ir neurons (maximal diameter 10–15 μm), whose processes were sometimes barely visible. These neurons were intermingled with a few larger, multipolar, and more darkly stained CB-ir cell bodies (maximal diameter 20–30 μm) that emitted three or four beaded dendrites. The Cl and VCl were largely devoid of CB-ir neuropil (Figs. 1, 3A, 8A).

DB and BST. The DB and BST were in continuity with the medial aspect of the VST at caudal levels (Figs. 1, 8, 9). The portion of the DB beneath the VST at levels 5 and 6 corresponds to the vertical limb of this structure (VDB; see Heimer et al., 1999), and, except for some CB-ir neurons, it was largely devoid of CB staining (Figs. 1, 8A, 9A). By contrast, this region stained for LAMP, and the intensity of the staining was stronger than that in the adjacent VST region (Figs. 1, 8B, 9B). The staining intensity for SP, AChE, CR, and ChAT in the VDB showed regional differences that were particularly obvious along its mediolateral extent (Fig. 9C–E) and in some cases resembled that displayed by the nearby VST (Fig. 9C–E). Clusters of large cell bodies immunopositive for CB, CR, and ChAT were scattered within the VDB (Fig. 9A,E,F). The ChAT-ir neurons outnumbered the CB- and CR-ir neurons and were embedded in numerous smooth and

TABLE 4. Relative Densities of Stained Neuropil[1] in the Nucleus Accumbens, Interface Islands, Claustrum, and Vertical Limb of the Diagonal Band in Human

	Neurochemical markers					
Basal forebrain structures	CB	LAMP	CR	SP	AChE	ChAT
Nucleus accumbens						
Core	++	++	+	+	++/+	++/+
Shell	+	++/+	+++	+++	++/+	++/+
Interface islands						
Alongside the ventral putamen	−	+++	++	+++	+++	++
Beneath the shell of Acb						
Small islands	+	+	+	+++	+++	+++
Large island	+	+	+++	+	+	+
Claustrum						
Dorsal claustrum	−	+++	++	−	−	−
Ventral claustrum	−	+++	++	−	−	−
Diagonal band (vertical limb)	−	++	++/+	++/+	++/+	++/+

[1]Density of stained neuropil: −, no staining; +, weak; ++, moderate; +++, intense. Acb, nucleus accumbens; CB, calbindin; LAMP, limbic system-associated membrane protein; CR, calretinin; SP, substance P; AChE, acetylcholinesterase; ChAT, choline acetyltransferase.

longitudinally oriented fibers also stained for ChAT (Fig. 9E,F). Other bundles of beaded fibers that stained for SP traversed this portion of the diagonal band along its mediolateral axis. The clusters of large cholinergic neurons that occurred in the VDB appeared, based on their location, to correspond to the Ch2 group of Mesulam and colleagues (1983). It is noteworthy that these clusters of ChAT-ir neurons occupied areas of the VDB that were completely free of LAMP immunostaining (Fig. 9B,E,F). Furthermore, a similar absence of LAMP immunostaining characterized the clusters of cholinergic neurons that were encountered at level 6 and that most likely represented the rostral pole of the nucleus basalis of Meynert (Fig. 11F–H).

The lateral division of the bed nucleus of the stria terminalis (BSTL) is already well delineated at level 5, where its rostral pole is continuous with the posteromedial sector of the VST (Fig. 1, 8A). At this level, the BSTL displayed an intense CR immunostaining, which was continuous with that of the caudal aspect of the VST (Figs. 1, 8C). Small CR-ir cell bodies were observed in the BSTL, but their dendrites could not been clearly visualized because of the intensity of background staining. A few CB-ir neurons were also scattered in a moderately stained neuropil (Figs. 1, 8A). The BSTL displayed a moderate immunostaining for LAMP and ChAT that was restricted to the neuropil (Figs. 1, 8B). Small areas containing numerous SP-ir varicose fibers and puncta, occasionally forming tubular profiles, occurred at the lateral aspect of the BSTL, but the rest of this structure was much more weakly stained (Figs. 1, 8D). An intense AChE staining was observed in a narrow streak located at the medial aspect of the BSTL, the rest of the structure being devoid of the enzyme.

DISCUSSION

This study has provided a detailed description of the distribution of some of the major chemical markers of the VST. Delineating this basal forebrain structure has always been a difficult task, particularly for the human brain (Holt et al., 1996, 1997; Lauer and Heinsen, 1996; Heimer et al., 1999; Morel et al., 2002; present study). Voorn and colleagues (1996) have described, based on the distribution of μ-opiate receptors, the human VST as being composed primarily of the Acb and the ventral part of the putamen, together with a ventral "transition zone," which comprises the portion of the head of the caudate nucleus that impinges upon the Acb. The border between the lateral Acb and the ventromedial extension of the putamen is difficult to trace; it represents a transitional zone called the *fundus putaminis* by Brockhaus (Lauer and Heinsen, 1996). The medial border of the Acb is formed by the rostral part of the insula magna, the major component of the islands of Calleja. It is continuous dorsally with the so-called *striatum gliosum subependymale*, an area that progressively replaces the caudate nucleus and that has been termed the *fundus caudati* by Brockhaus (Lauer and Heinsen, 1996).

One of the major problems in delineating the VST resides in the difficulties in establishing clearcut borders of its major component, the Acb. To determine the full rostrocaudal extent of the VST and the Acb, the human VST has been subdivided into six levels extending rostrocaudally from the rostral tip of the striatum to the level at which the basal nucleus of Meynert appears. By combining several markers and comparing their distribution over the full rostrocaudal extent of the VST, the present study has yielded a more comprehensive view of the chemical organization of that striatal region. We have also provided information on the neurochemical characterization of other basal forebrain structures that surround the VST, such as the interface islands, the Cl, the DB, and the BST. The functional significance of these results is discussed below in light of similar data gathered for several species.

Rostral aspect of the VST

The rostroventral part of the caudate nucleus and putamen is considered a component of the VST in primates (Holt et al., 1996, 1997; Haber and McFarland, 1999; Heimer et al., 1999; Haber et al., 2000). In macaque monkeys, this region receives inputs from the orbitofrontal cortex and medial frontal-anterior cingulate cortex (Eblen and Graybiel, 1995) and is viewed as a transition zone (or "prelimbic striatum") between the dorsal caudate nucleus-putamen and the Acb. Furthermore, the ventromedial sector of the caudate nucleus is considered, based on its afferents from the orbital and medial prefrontal cortex and the amygdaloid complex, an interface between the shell of the Acb and the rest of the VST (Fudge et al., 2002). Recently, the rostroventral part of human caudate nucleus and putamen has been included in the so-called T3 striatal territory, as defined by Morel and colleagues.

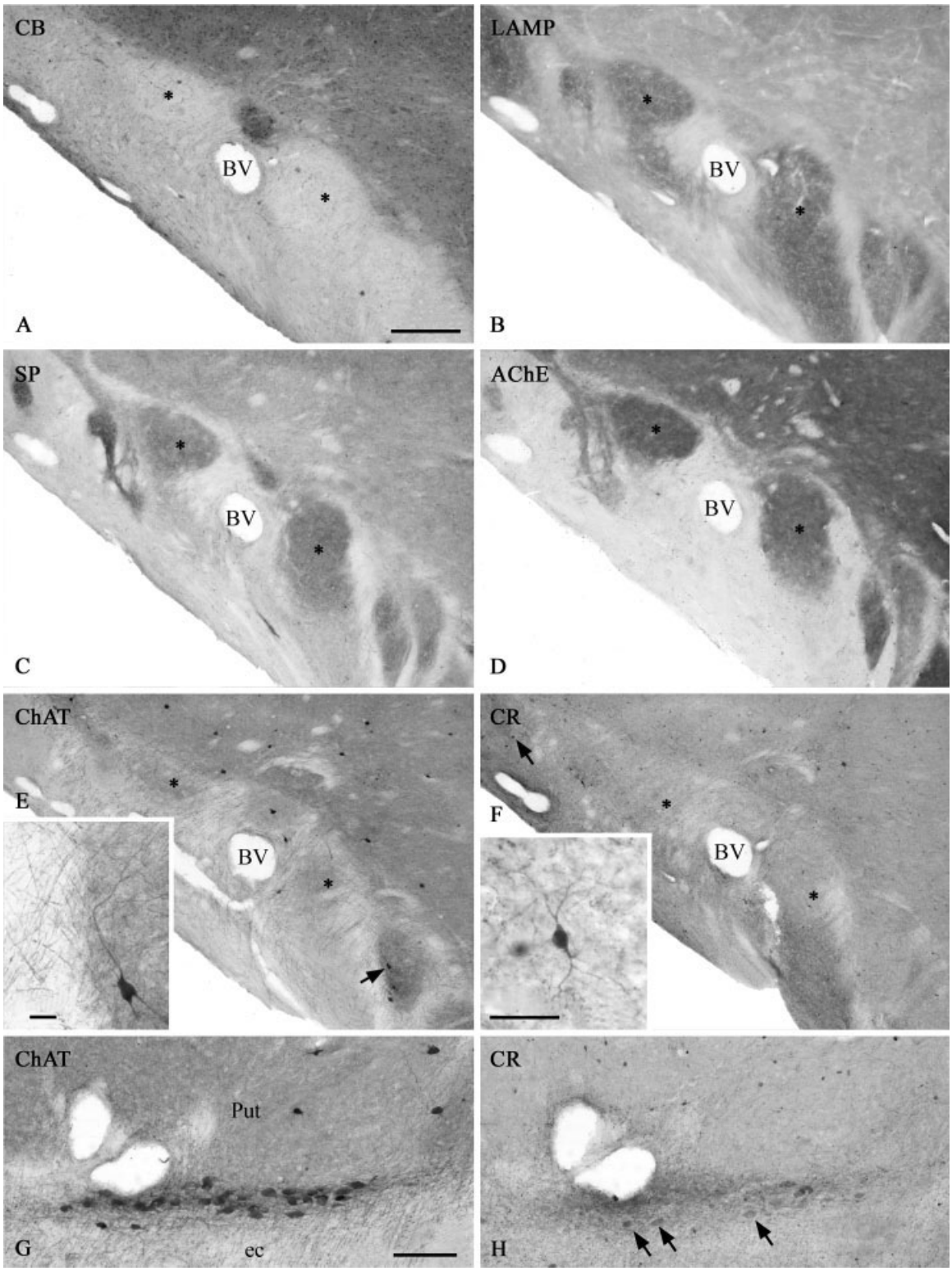

Fig. 7. **A–F:** Photomicrographs illustrating the immunostaining patterns of the interface islands located along the ventral putamen and its border with the external capsule. The exact location of this field is indicated in Figure 3D. The asterisks mark two islands located close to a blood vessel (BV). The arrow in E points to a cholinergic neuron located in one of these islands. This neuron is shown at a higher magnification in the **inset** in E. Arrow in F points to the CR-ir neuron that is shown in the **inset** in F. **G:** Example of a cluster of ChAT-ir neurons located at the interface between the putamen (Put) and the external capsule (ec). **H:** The same cluster harbors some large CR-ir neurons (arrows), as seen in an adjacent section. Scale bar = 500 μm in A, in E,F = 50 μm, in G = 200 μm.

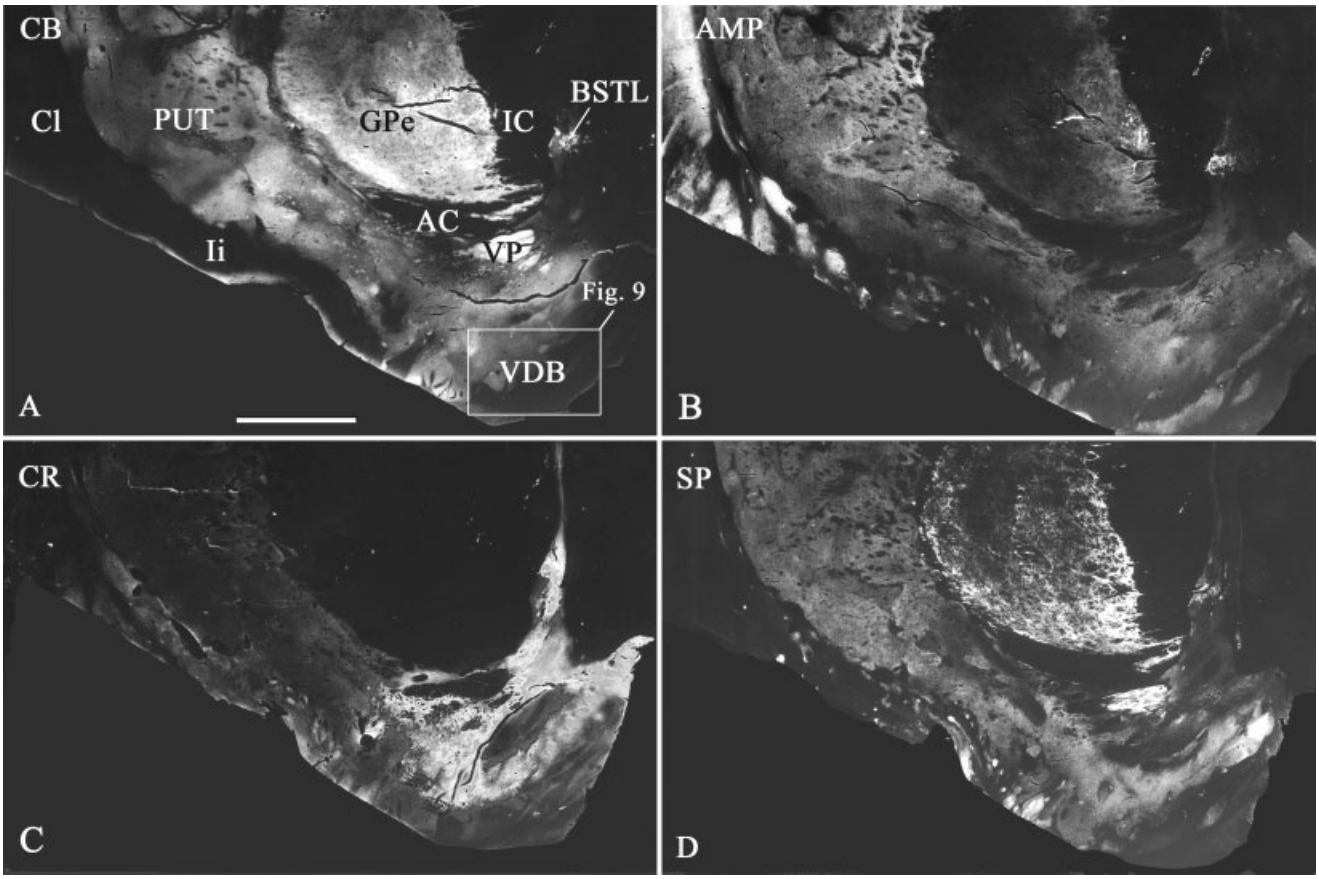

Fig. 8. **A–D:** Direct prints of the VST, as seen in adjacent sections stained for CB, LAMP, CR, and SP. The plane of section corresponds to level 5 in Figure 1. The area delimited by the box in A is shown at higher magnification in Figure 9. Scale bar = 5 mm.

(2002), a sector that corresponds to the paralimbic striatal territory, as defined by Mesulam (1985).

The rostroventral parts of the caudate nucleus and putamen in humans has been characterized by intense CR immunoreactivity in or around CB-poor patches (Morel et al., 2002). In our study, CB-poor patches were found to correspond to zones of intense CR immunostaining in the ventromedial sector of the striatum. Furthermore, the CB-poor patches in the rostroventral striatal regions expressed LAMP but not SP. Because of their intense CR immunostaining, these CB-poor patches may be part of the most rostral extensions of the shell of the Acb, which has been reported to express high levels of CR immunoreactivity in rats and monkeys (Seifert et al., 1998; Brauer et al., 2000). However, similar CR-rich patches located more caudally in the shell were intensely stained for SP but not for LAMP, a staining pattern opposite to what is seen more rostrally. This variation in staining patterns suggests that the chemical makeup of the shell may vary along its rostrocaudal axis. However, it is also possible that the rostral patches of the ventromedial striatum do not really belong to the shell but represent a distinct entity.

The idea that the rostral pole of the Acb might be an entity distinct from the shell and core has been advocated on the basis of its distinct efferent projections in rodents (Zahm and Brog, 1992; Zahm and Heimer, 1993). However, other authors have considered the rostral pole of the Acb as part of the shell (Meredith et al., 1993). In human and nonhuman primates, the rostral pole of the Acb could not always be recognized as such (Ikemoto et al., 1995; Meredith et al., 1996). However, allusion to a "rostral subdivision" of the Acb was made for monkeys based on the fact that its content in transmitters and peptides was similar to that of the main part of the Acb (Ikemoto et al., 1996). Our data reveal that the rostral portion of the VST in humans displays immunostaining patterns that are much more complex than those in other species. Furthermore, our results show that there is, at present, no reliable marker that could help in defining the border between the dorsal striatum and the Acb as well as the core/shell dichotomy at the most rostral levels of the VST. Serial reconstruction studies with a single marker (e.g., CB or LAMP) could help in determining whether the patches in the VST form a continuous or interrupted compartment. This type of information would facilitate the interpretation of the incongruity in the distribution of the same marker noted in the present study.

Core and shell regions of the Acb

In primates, the Acb merges imperceptibly with the rostroventral parts of the caudate nucleus and putamen.

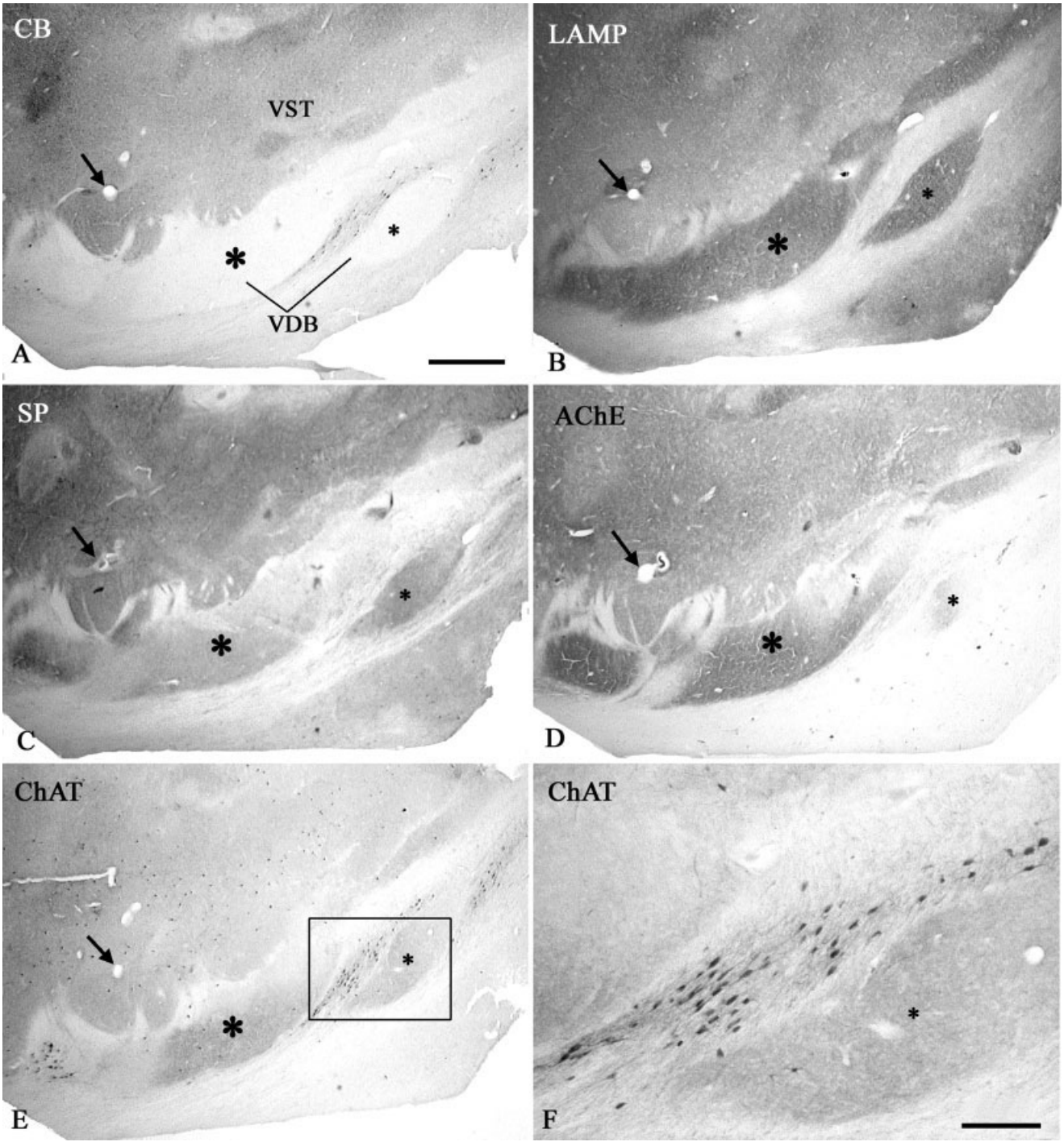

Fig. 9. **A–F:** Photomicrographs illustrating the staining patterns for CB, LAMP, SP, AChE, and ChAT in the portion of the vertical limb of the diagonal band (VDB) that lies below the VST at level 5. The location of this field is indicated in Figure 8A. Large and small asterisks mark corresponding areas of the VDB in the different photomicrographs, and arrows point to a blood vessel that serves as a landmark. The area delimited by the box in E is shown at a higher magnification in F. The latter illustrates some cholinergic cell bodies in this portion of the VDB, which is completely devoid of LAMP immunostaining (see B). Scale bar = 1 mm in A, in F = 250 μm.

Its complex immunostaining is characterized by an absence of simple relationships among the different markers (Haber et al., 1990; Martin et al., 1991; Côté et al., 1995; Holt et al., 1996, 1997; Prensa et al., 1999; Heimer et al., 1999; Morel et al., 2002; present study). For humans, we observed a marked change from a mosaic pattern typical of that of the rostral striatum to a more uniform distribution in Acb at mid-VST level (levels 3 and 4). At these

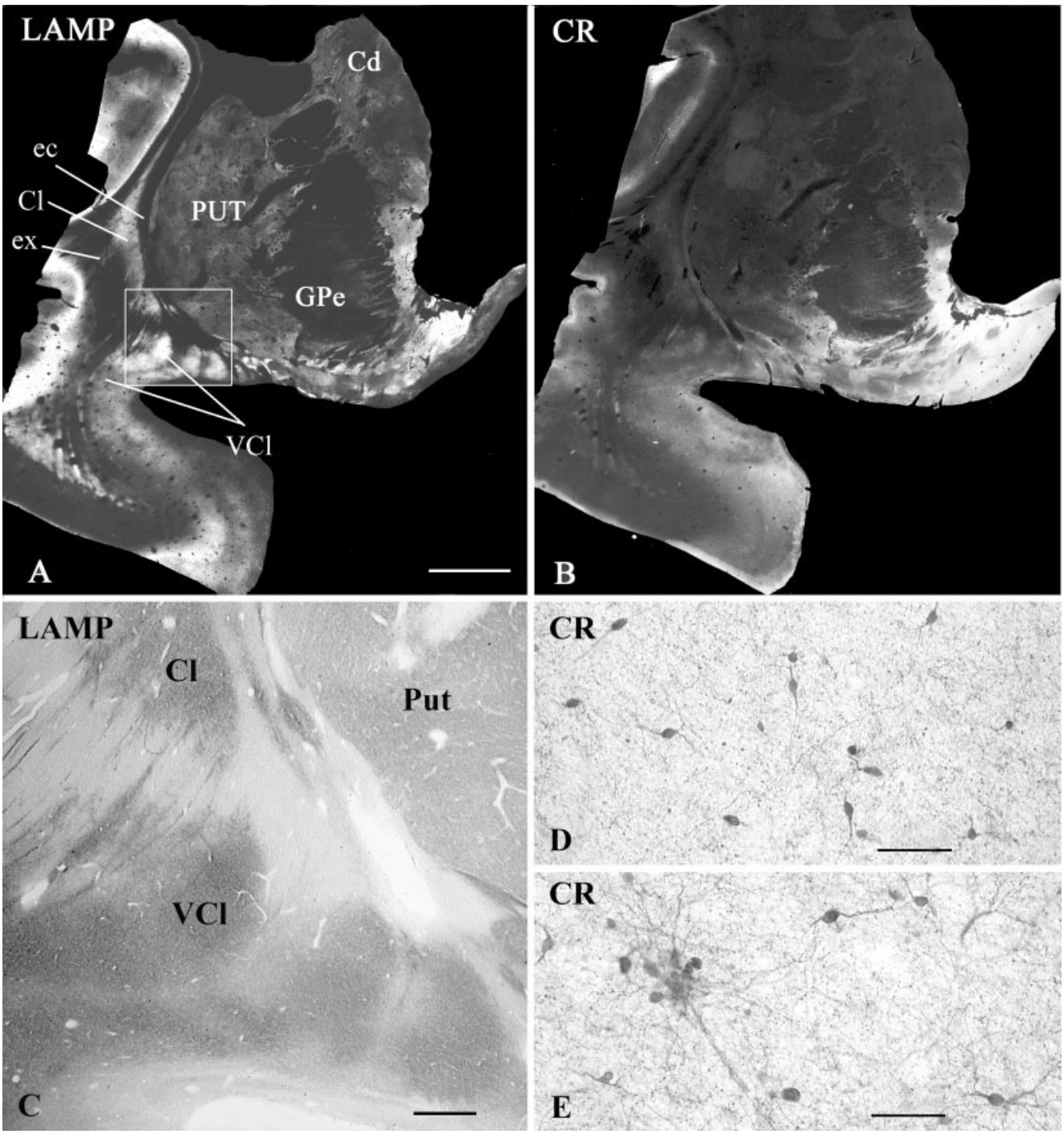

Fig. 10. **A,B:** Direct prints of two adjacent sections through the rostral striatum stained for LAMP (A) and for CR (B). The plane of section corresponds to levels 5 in Figure 1. **C:** Photomicrograph showing LAMP immunoreactivity in both the dorsal (Cl) and the ventral divisions (VCl) of the claustrum (see box in A). **D,E:** High-power view of some typical CR-ir neurons in the dorsal claustrum (D) and ventral claustrum (E). Scale bar = 5 mm in A, in C = 1 mm, in D,E = 50 μm.

levels, the shell can be readily identified as a ventromedial region weakly stained for CB but markedly enriched in CR and SP. This neurochemical pattern appears similar to that previously described for rats and monkeys (Voorn et al., 1989; Ikemoto et al., 1995; Meredith et al., 1996; Brauer et al., 2000). However, the boundaries between the core and the shell regions, as delimited by the different markers used in the present study, do not match perfectly in the human Acb. Previous studies in human have shown that AChE can be used reliably to delimit the core from

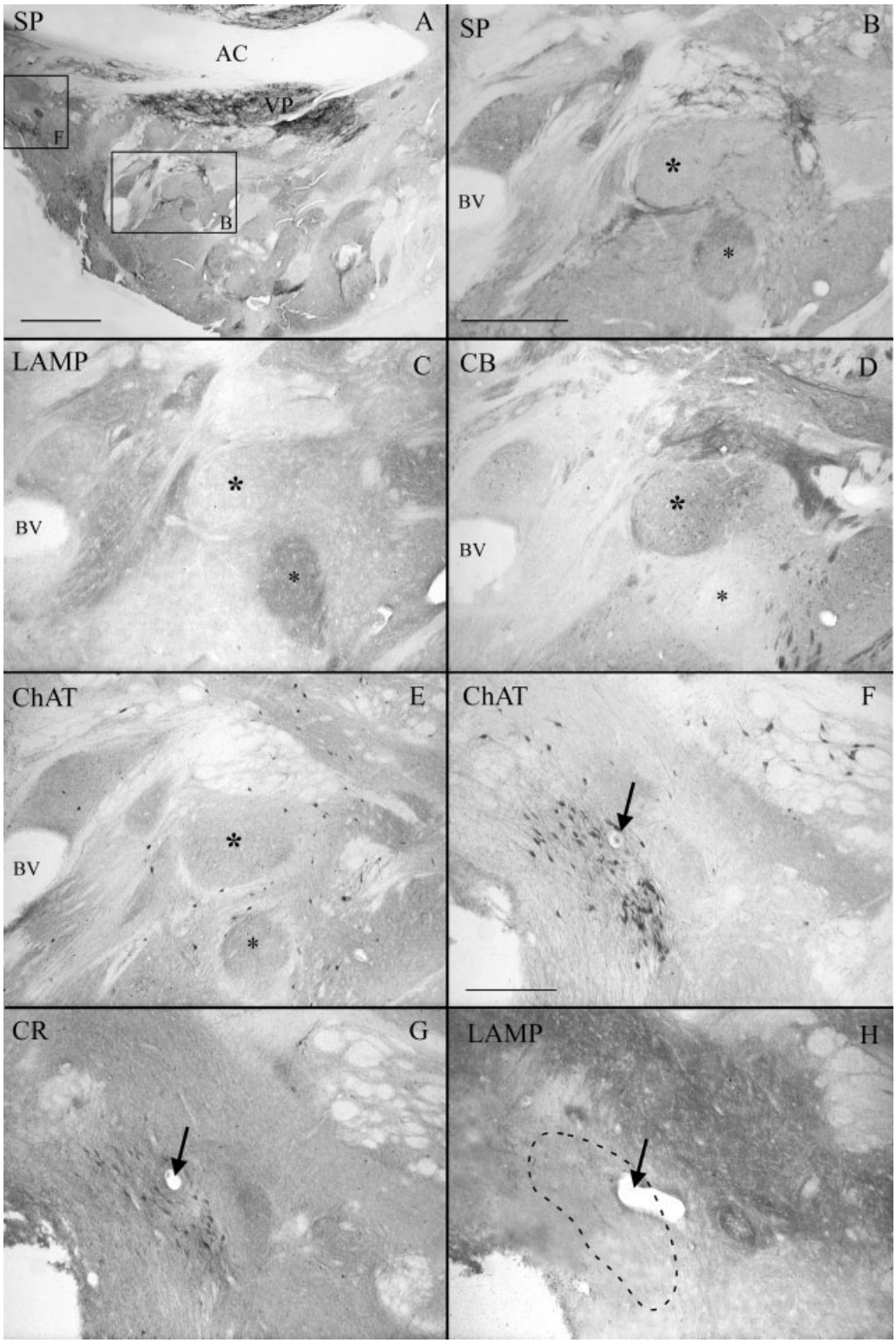

Fig. 11. Photomicrographs illustrating immunostaining for SP, LAMP, CB, ChAT, and CR in the VST at level 6 (see Fig. 1). **A:** Low-power view of the SP immunoreactivity displayed by the ventral pallidum (VP) and surrounding striatal tissue. **B–E:** High-power views of the area of the VST that is enclosed by box B in A. This field is shown in adjacent sections stained for SP, LAMP, CB, and ChAT. Large and small asterisks indicate corresponding areas in the different sections. Note the CB-rich area (large asterisk in D), which lie close to a CB-negative zone (small asterisk); both regions express opposite patterns of staining for LAMP and SP but are equally enriched in ChAT-ir neuropil. **F–H:** High-power view of the area of the striatum enclosed by box F in A. This field is shown in adjacent sections stained for ChAT, CR, and LAMP. Arrows point to a blood vessel that serves as a landmark. Note the clusters of ChAT- and CR-ir neurons (F,G) that occur at this level, as well as the absence of LAMP immunostaining in the area occupied by these clusters (dashed line in H). Scale bar = 2 mm in A, in B,F = 500 μm.

the shell, the shell being more intensely stained than the core for this enzyme (Zaborszky et al., 1985; Voorn et al., 1994). In our AChE material, however, clear boundaries between the two subdivisions of the Acb could not be clearly established, and AChE-rich areas were found to intermingle with AChE-poor areas in both subdivisions of the nucleus.

The distribution of LAMP in the Acb was also complex. For example, LAMP immunostaining was present in the ventromedial CB-poor shell at level 3 but absent at level 4, indicating that the shell is chemically heterogeneous. The lack of LAMP in the caudal part of the shell is consistent with the existence of a ventromedial region of the VST that involves part of the Acb and stains more weakly for LAMP than the rest of the structure in monkeys (Côté et al., 1995). The absence of LAMP in the caudal aspect of the shell is surprising in that, by virtue of its extensive connections with limbic circuits, the shell is considered the "limbic" part of the Acb (Mogenson et al., 1980; Groenewegen and Russchen, 1984; Heimer et al., 1991; Mogenson and Yang, 1991).

The core of the human Acb was found to display an intense CB immunostaining that involves both cell bodies and neuropil and is comparable to that of the extrastrisomal matrix of the caudate nucleus and putamen. However, this portion of the Acb expresses a staining for LAMP that resembles that of the dorsally located striosomes (Prensa et al., 1999). This surprising finding suggests that the core of the Acb might receive limbic afferents similar to those innervating the dorsally located striosomes. In any event, the fact that the core and shell display opposite patterns of LAMP immunostaining supports the current belief that these two regions of the Acb are separate functional entities. In this perspective, the ChAT-ir neurons located at the boundary between the core and the shell with dendrites that extend into the two compartments, as shown in this study, could play an important role in the communication between the two major subdivisions of the Acb.

The shell appears to be also chemically heterogeneous along its mediolateral extent. As in monkeys, the CR-ir neuropil of the shell in humans is more intense dorsomedially than laterally (Brauer et al., 2000; present study). Furthermore, the CR-ir neuropil displays a marked mediolaterally decreasing gradient in the human shell. This distribution pattern might reflect the arrangement of input from the paraventricular thalamic nucleus, which contains CR-ir neurons that project to this subdivision of the Acb (Berendse and Groenewegen, 1990; Resibois and Rogers, 1992; Moga et al., 1995; Bubser et al., 2001).

Unlike the case with CR, CB immunostaining is much more intense in the lateral than in the dorsomedial aspect of the human shell. A similar mediolateral heterogeneity in the CB immunostaining of the shell has been reported for rodents (Jongen-Relo et al., 1994; Meredith et al., 1996). Likewise, mediolateral differences in SP, Leuenkephalin, dopamine, and neurotensin immunoreactivity and AChE staining in the shell have been reported for different species (Zaborszky et al., 1985; Zahm and Heimer, 1988; Voorn et al., 1989; Zahm and Brog, 1992; present study). A homologue of the ChAT-rich medial zone of the shell of the rat Acb (Phelps and Vaughn, 1986) could not be found in the present material (see also Holt et al., 1996). It is possible, however, that the ChAT-rich granular islands that lie below the medial aspect of the shell are equivalent to the ChAT-immunostained region noted for the rodent Acb.

Our results show that the ChAT-ir cell bodies are rather uniformly distributed throughout the shell and core of the Acb, so that this structure cannot be distinguished from the ventral one-third of the putamen on such a basis. These data are at variance with those reported previously for monkeys, in which the density of cholinergic neurons was reportedly lower in the shell than in the core (Brauer et al., 2000) and lower in the dorsal striatum than in the Acb (Mesulam et al., 1984). In rats, however, the cholinergic neurons are more numerous in the shell than in the core (Meredith et al., 1989). In contrast to the ChAT-ir cells, neurons stained for CR were heterogeneously distributed in the human Acb, with a marked mediolaterally increasing gradient. This finding contrasts with results reported for rats, in which no significant differences in the densities of the CR-ir neurons were found between the two subdivisions of the Acb (Hussain et al., 1996).

There also exist discrepancies with respect to the size of the cholinergic neurons present in the dorsal striatum vs. those located in the Acb in human and nonhuman primates. Some investigators reported that cholinergic neurons in the Acb are significantly smaller than those located in the dorsal striatum (Mesulam et al., 1984; Lehericy et al., 1989; Holt et al., 1996; Brauer et al., 2000), whereas others saw no difference (Geula et al., 1990; Selden et al., 1994). In the present study, ChAT-ir neurons in the Acb were slightly smaller and more poorly branched than those in the dorsal striatum, an observation that also applies to the large CR-ir neurons. By contrast, the size and morphological features of the medium-sized CR-ir neurons in the Acb did not differ from those in the dorsal striatum. We also found that the ChAT-ir neurons and the large CR-ir neurons located in the shell were smaller than those in the core of the human Acb. The latter finding is the opposite of the results obtained for cholinergic neurons in the rhesus monkey (Brauer et al., 2000) but is congruent with the data reported for rats (Meredith et al., 1993).

We also found size differences in ChAT- and CR-ir neurons along the mediolateral extent of the shell and core of the human Acb, neurons in the medial halves of both subdivisions being smaller than those in the lateral halves. Also worth noting is the fact that the medial half of the shell is devoid of large CR-ir neurons but harbors large ChAT-ir neurons and medium-sized CR-ir neurons. Interestingly, the same type of neuronal arrangement occurs in the ventrally located patches that characterize the most rostral portion of the VST (levels 1 and 2) and might be rostral extensions of the human Acb.

Caudal aspect of the VST

Caudally, the medial part of the shell, sometimes referred to as the *septal* pole or the *cone* region (Groenewegen et al., 1990, 1991), is contiguous dorsally with the lateral part of the BST. Ventrally, it merges imperceptibly with other components of the basal forebrain, including the ventral pallidum (VP) and the rostral subcommissural substantia innominata (SI). The most remarkable feature of this caudal sector of the VST is the increasing amount of CR immunostaining, which tends to spread over a large extension of the VST that is mostly devoid of CB. This pattern of immunostaining supports the suggestion made earlier by Meredith et al. (1996) that most of the caudal aspect of the Acb is occupied by the shell. The boundary

between the VST and the more posterior part of the basal forebrain is not clearly defined but can be estimated by the transition to more uniform CR immunostaining and the appearance of the basal nucleus of Meynert (Morel et al., 2002; present study). In rats, the most caudal part of the shell receives a dense noradrenergic innervation, whereas the rostral aspect of the shell, the entire extent of the core, and the dorsal striatum are devoid of such innervation (Berridge et al., 1997).

The histochemical heterogeneity of the VST increases substantially at caudal levels because of the intermingling of large pallidal neurons with the medium-sized striatal neurons. At level 6, most of the region that has traditionally been referred to as the *subcommissural SI* is occupied by ventral striatal and ventral pallidal territories, the latter displaying a very dense SP immunoreactivity. In contrast to the case in the VST, the distribution pattern of SP immunoreactivity in the SI corresponds largely to that seen in AChE-stained material (Pioro et al., 1990). Other parts of this subcommissural area are occupied by clusters of large cholinergic neurons that belong to the basal nucleus of Meynert (group Ch4 of Mesulam et al., 1983) and the vertical limb of DB (group Ch2 of Mesulam et al., 1983). The present study has shown that these cholinergic neurons occupy areas of the basal forebrain that are devoid of LAMP immunostaining, a finding that is in agreement with previous results gathered for monkeys (Côté et al., 1996).

Forebrain structures adjacent to VST

Interface islands. Numerous compact clusters of small neurons widely dispersed in the basal forebrain and prevailing where major nuclear structures abut one another have been previously reported for humans (Voorn et al., 1996; Heimer et al., 1999). The exact functional significance of these islands is unknown (Voorn et al., 1996; Lauer and Heinsen, 1996; Heimer et al., 1999), but it has been recently suggested that structural abnormalities in these, also called *interface islands,* may be involved in the etiology of schizophrenia (Heimer, 2000). The term *neurochemically unique domains in the Acb and putamen* (NUDAP) was used to define a subtype of cellular islands in humans that displays high binding densities for the μ and κ opiate receptors, D1 dopamine receptors, and AChE activity and forms a continuous sheet that surrounds the entire ventral border of the Acb and the ventral one-third of the putamen (Voorn et al., 1994, 1996). These cellular islands can be distinguished from the islands of Calleja on the basis of the size of their cell bodies (Voorn et al., 1996) and the lack of dopamine D3 receptor (Voorn et al., 1994), which is a reliable marker for the islands of Calleja (Landwehrmeyer et al., 1993; Murray et al., 1994). The ring of cellular islands that surrounds the Acb is thought to be part of the shell division of this structure (Voorn et al., 1996), an idea that agrees with other data gathered for human (Lauer and Heinsen, 1996). However, the cell density in the NUDAP is higher than that in the contiguous part of the shell subdivision of the Acb (Voorn et al., 1996). Recently, NUDAPs have also been recognized in nonhuman primates by their richness in μ opiate receptor-binding sites (Daunais et al., 2001).

The neurochemical features of the cellular islands that surround the human VST were partially characterized by Heimer and colleagues (1999). These authors have identified two types of such islands: 1) the granular islands, which contain predominantly very small "glia-like" or granular neurons, and 2) the parvicellular islands, which contain somewhat larger neurons, the majority of which are, however, still significantly smaller than the regular striatal neurons. The granular cell islands are similar to the "islands of Calleja" of macrosmatic mammals and are readily identifiable in all mammalian species, including humans (Meyer et al., 1989), although there exist considerable interspecies differences with regard to their distribution (Alheid et al., 1990). Both types of islands showed moderate to strong AChE staining but differed in their SP immunoreactivity.

In the present study, several islands surrounding the human VST could be distinguished from striatal tissue, particularly by their lack of CB immunostaining. The islands located at the lateral rim of the putamen are likely, based on their location and pattern of AChE and SP staining, to correspond to the granular interface islands distributed alongside the ventral putamen (Heimer et al., 1999). We found these islands, apart from their intense AChE and SP staining, to be markedly enriched in LAMP protein. Furthermore, the intensity of the LAMP staining in these islands was stronger than anywhere else in the striatal tissue, including the entire VST and the dorsally located striosomes (Prensa et al., 1999). Although the exact functional role of these basal forebrain structures remains unknown, this finding suggests a close association of these islands with limbic system circuitry. These islands also contain ChAT- and CR-ir neurons embedded within a moderate neuropil. These novel findings do not support the common belief that the granular islands are devoid of intrinsic cholinergic neurons (Phelps and Vaughn, 1986; Wahle and Meyer, 1986; Talbot et al., 1988; Heimer et al., 1999). Furthermore, groups of large ChAT-ir neurons were disclosed at the interface between the ventral putamen and the external capsule. These cells could represent displaced elements of the basal nucleus of Meynert, which is believed to invade the VST at points where this structure borders on the external capsule or the core of the ventral pallidum (Heimer et al., 1999).

An insula magna located at the medial edge of the Acb has been found in all species examined thus far, including humans (Meyer et al., 1989; Heimer et al., 1999). This voluminous island is populated by neurons somewhat larger than those of the granular cell clusters and is thus considered part of the parvicellular island group (Heimer et al., 1999). Unlike the granular islands, the insula magna is largely devoid of SP (Heimer et al., 1999). Judged by its size and weak SP immunoreactivity, the large island observed at the medial aspect of the Acb in the present study appears to correspond to the insula magna that occurs in other species. The neuropil of this island is markedly enriched in CR but largely devoid of ChAT. It is worth noting that, in contrast to the interface islands encountered along the lateral border of the ventral putamen, the islands that fringe the shell of the Acb are only weakly stained for LAMP. This finding indicates that the group of interface islands surrounding the VST and the ventral putamen are functionally heterogeneous. Furthermore, our data suggest that the ChAT-ir neurons inserted between the cellular islands and the VST might act as a functional interface between these two basal forebrain structures.

Claustrum. This sheet of gray matter inserted between the extreme capsule laterally and the external cap-

sule medially is reciprocally and topographically linked with sensory, motor, and "association" areas of the cerebral cortex (Sherk, 1986; Baizer et al., 1997). Although anatomical and electrophysiological data support the idea of a functional specialization in different regions of the claustrum (Shima et al., 1996), no differences in the chemical features have been observed along the extent of this structure (Reynhout and Baizer, 1999; Baizer, 2001).

The present study has provided the first evidence that, although functionally distinct (Sherk, 1986; Shima et al., 1996; Baizer et al., 1997), the dorsal and ventral subdivisions of the claustrum display a very intense and homogeneous immunostaining for LAMP in humans. The origin and the functional role of this glycoprotein in the claustrum are unknown. However, it must be mentioned that the heaviest projection from the amygdala to the claustrum arises from the magnocellular division of the basal nucleus (Majak et al., 2002), which is highly immunoreactive for LAMP (Côté et al., 1996). It is thus possible that the LAMP immunostaining observed in the human claustrum belongs to fiber terminals of this amygdaloclaustral projection. Furthermore, the fact that the intensity of the staining for LAMP in the claustrum is similar to that displayed by the interfaced islands alongside the ventral putamen raises the possibility that these basal forebrain structures participate in the same limbic microcircuitry.

Our results support the idea that the subdivision of the claustrum into functional compartments is not associated with variations in neuronal morphology or immunostaining for calcium binding proteins (Brand, 1981; Sherk, 1986; Reynhout and Baizer, 1999). The present study has demonstrated the existence of two types of CR-ir neurons and two types of CB-ir neurons that are homogeneously distributed in the human claustrum. In monkeys, the claustrum was reported to contain only a single type of CR-ir neurons that are characteristically aligned in parallel (Reynhout and Baizer, 1999). Here, the human claustrum was found to contain both medium-sized and large CR-ir neurons, and each of these cell types was rather uniformly scattered throughout the structure. In contrast, the CB immunostaining appears to follow a similar pattern of distribution in human and nonhuman primates. It is much lighter than that of CR and involves numerous small and a few larger neurons that are uniformly scattered throughout the claustrum (Reynhout and Baizer, 1999; present study). Hence, the primate claustrum appears to differs from its rodent homologue, which is apparently devoid of CB-ir neurons (Druga et al., 1993).

DB and BST. The VDB and the rostral end of the BSTL are in continuity with the posteromedial portion of the VST. The BST was originally included into Brockhaus' definition of the fundus striati (Brockhaus, 1942), but this structure is currently considered a key component of the "extended amygdala." The latter term refers to a group of anatomically and functionally related structures that extends rostrocaudally from the BST to the centromedial nucleus of the amygdala (Johnston, 1923; de Olmos et al., 1985; Alheid and Heimer, 1988; Heimer and Alheid, 1991; Alheid et al., 1995) and has been implicated in a number of motivational behavioral processes (Davis and Shi, 1999; Koob, 1999).

The entire human VDB and the portion of the BSTL included in the most caudal levels examined here were found to stain for LAMP. This finding agrees with the fact that LAMP stains the entire extended amygdala in nonhuman primates (Côté et al., 1996). However, further studies are needed to establish that LAMP is a reliable marker for the entire extended amygdala in humans. The significance of the presence of LAMP in these structures is presently unknown. By virtue of its function as a cell adhesion molecule, LAMP is believed to mediate the formation of specific pathways during development (Keller et al., 1989). This protein might thus play an important role in establishing and maintaining various limbic system connections that are related either directly or indirectly to the DB and the BST. However, the fact that cholinergic neurons in the VDB do not express LAMP indicates that this protein is not the only cell adhesion molecule involved in the establishment of limbic system connections.

The horizontal and vertical limbs of the DB and the basal nucleus of Meynert form an aggregate of neurons that traverses the basal forebrain obliquely between its rostromedial and caudolateral regions (de Lacalle and Saper, 1997; Heimer et al., 1999). The DB is known to harbor a large number of cholinergic neurons as well as neurons that contain parvalbumin, CR, or CB. In rodents, neurons containing calcium-binding proteins are distinct from the cholinergic neurons (Kiss et al., 1997), whereas, in monkeys, most of the ChAT-ir neurons express CB (Ichitani et al., 1993; Geula et al., 1993). Here, numerous ChAT- and CB-ir neurons, as well as some CR-ir cell bodies, were scattered within the human VDB. However, colocalization studies are needed to determine whether these neurons belong to a single cell population or various cell populations.

Functional considerations

The VST receives inputs from various limbic structures (Russchen et al., 1985; Haber et al., 1990, 1995, 2000; Friedman et al., 2002) and is thought to be involved in reward and goal-directed behavior (Burns et al., 1996; Robbins and Everitt, 1996). Its major component, the Acb, is considered a neural substrate for limbic–motor interactions (Mogenson et al., 1980, 1993; Groenewegen et al., 1996). The Acb is a nodal point in the so-called ventral striatopallidal system; it receives afferents related to affective and motivational states and arising from limbic structures, such as the amygdala, hippocampus, prefrontal cortex, midbrain monoamine systems, and brainstem autonomic centers (Kelley et al., 1982; Kelley and Domesick, 1982; McDonald, 1991; Brog et al., 1993; Haber et al., 2000). It also has extensive connections with skeletal motor and visceral motor output systems (Nauta et al., 1978; Groenewegen and Russchen, 1984; Heimer et al., 1991). More recently, the Acb has been considered to be a key component of the so-called brain-reward circuitry, which mediates motivated behavior (Schultz et al., 1992, 1997; Robbins and Everitt, 1996; Breiter et al., 1997; Breiter and Rosen, 1999). Disturbances at this level have been implicated in a number of affective disorders, such as schizophrenia and drug abuse (Koob, 1992; Robbins and Everitt, 1996). Recent functional imaging investigations in humans have shown that the Acb is activated in situations related to drug-associated reward (Breiter et al., 1997; Stein et al., 1998) and/or monetary reward (Elliot et al., 2000; Breiter et al., 2001).

Our data reveal that the core and shell divisions of the human Acb differ in their chemical compositions. This finding concurs with the idea that they represent distinct but interconnected functional domains, as is the case in

rats and monkeys (Zahm and Brog, 1992; Kelley, 1999; Zahm, 1999; Haber et al., 2000; Reynolds and Berridge, 2001; Ikemoto, 2002). We showed that both shell and core are immunoreactive for LAMP, although this staining is distributed in a rather complex fashion. This heterogeneous labeling might reflect differences in the density of terminals from limbic structures, such as the amygdaloid complex and the hippocampus. In nonhuman primates, the basal amygdaloid nucleus is one of the major inputs to the Acb (Russchen et al., 1985; Friedman et al., 2002; Fudge et al., 2002) and is highly immunoreactive for LAMP (Côté et al., 1996). Furthermore, the magnocellular and intermediate divisions of the basal nucleus are the main sources of projections to the shell, whereas the parvicellular division innervates the shell and the core (Friedman et al., 2002). Since these three subdivisions of the basal nucleus express LAMP (Côté et al., 1996), it is possible that the LAMP staining observed in the shell and the core reflects the projections from this amygdaloid nucleus upon the human Acb. Another source of limbic projections to the Acb is the hippocampal formation, which also stains positively for LAMP and targets preferentially the shell region (Côté et al., 1996; Friedman et al., 2002).

We also found the shell portion of the Acb to be chemically heterogeneous along its mediolateral and rostrocaudal extents in humans, as in rats and monkeys. Such heterogeneities could be due to differences in anatomical connections (Phillipson and Griffiths, 1985; Zahm and Brog, 1992; Brog et al., 1993; Voorn et al., 1994; Jongen-Relo et al., 1994; Brauer et al., 2000; Fudge et al., 2002; Ikemoto, 2002). Recent functional imaging investigations have shown that the rostral and caudal portions of this accumbal region play distinct functional roles. For example, $GABA_A$ receptor activation in the rostral part of the shell of rodents produces appetitive eating behavior, whereas defensive treading behavior is obtained when the caudal part of the shell is involved (Reynolds and Berridge, 2001). Hence, the results of anatomical, immunohistochemical, and imaging studies in rats, monkeys, and humans indicate that the VST is a strikingly complex and functionally heterogeneous structure. The normative data gathered in the present study could help in interpreting the variation of activity that occurs in the human VST under both normal and pathological conditions.

ACKNOWLEDGMENTS

The authors thank Martin Lévesque for his help with the illustrations. We also thank Dr. Pat Levitt for his generous gift of LAMP antibodies, Dr. Michel Marois for providing the postmortem material and Martin Lévesque for his help with the illustrations.

LITERATURE CITED

Alheid GF, Heimer L. 1988. New perspectives in basal forebrain organization of special relevance for neuropsychiatric disorders: the striatopallidal, amygdaloid, and corticopetal components of substantia innominata. Neuroscience 27:1–39.

Alheid GF, Heimer L, Robert CS. 1990. Basal ganglia. In: Paxinos G, editor. The human nervous system. San Diego: Academic Press. p 483–582.

Alheid GF, de Olmos JS, Beltramino CA. 1995. Amygdala and extended amygdala. In: Paxinos G, editor. The rat nervous system. San Diego: Academic Press. p 495–578.

Baizer JS. 2001. Serotonergic innervation of the primate claustrum. Brain Res Bull 55:431–434.

Baizer JS, Lock TM, Youakim M. 1997. Projections from the claustrum to the prelunate gyrus in the monkey. Exp Brain Res 113:564–568.

Berendse HW, Groenewegen HJ. 1990. Organization of the thalamostriatal projections in the rat, with special emphasis on the ventral striatum. J Comp Neurol 299:187–228.

Berridge CW, Stratford TL, Foote SL, Kelley AE. 1997. Distribution of dopamine beta-hydroxylase-like immunoreactive fibers within the shell subregion of the nucleus accumbens. Synapse 27:230–241.

Brand S. 1981. A serial section Golgi analysis of the primate claustrum. Anat Embryol 162:475–488.

Brauer K, Hausser M, Hartig W, Arendt T. 2000. The core-shell dichotomy of nucleus accumbens in the rhesus monkey as revealed by double-immunofluorescence and morphology of cholinergic interneurons. Brain Res 858:151–162.

Breiter HC, Rosen BR. 1999. Functional magnetic resonance imaging of brain reward circuitry in the human. Ann N Y Acad Sci 877:523–547.

Breiter HC, Gollub RL, Weisskoff RM, Kennedy DN, Makris N, Berke JD, Goodman JM, Kantor HL, Gastfriend DR, Piorden JP, Mathew RT, Rosen BR, Hyman SE. 1997. Acute effects of cocaine on human brain activity and emotion. Neuron 19:591–611.

Breiter HC, Aharon I, Kahneman D, Dale A, Shizgal P. 2001. Functional imaging of neural responses to expectancy and experience of monetary gains and losses. Neuron 30:619–39.

Brockhaus H. 1942. Zur feineren Anatomie des Septum und des Striatum. J Psychol Neurol 51:1–56.

Brog JS, Salyapongse A, Deutch AY, Zahm DS. 1993. The patterns of afferent innervation of the core and shell in the "accumbens" part of the rat ventral striatum: immunohistochemical detection of retrogradely transported fluoro-gold. J Comp Neurol 338:255–278.

Bubser M, Backstrom JR, Sanders-Bush E, Roth BL, Deutch AY. 2001. Distribution of serotonin 5-HT(2A) receptors in afferents of the rat striatum. Synapse 39:297–304.

Burns LH, Annett L, Kelley AE, Everitt BJ, Robbins TW. 1996. Effects of lesions to amygdala, ventral subiculum, medial prefrontal cortex, and nucleus accumbens on the reaction to novelty: implication for limbic-striatal interactions. Behav Neurosci 110:60–73.

Celio MR. 1990. Calbindin D-28k and parvalbumin in the rat nervous system. Neuroscience 35:375–475.

Côté PY, Levitt P, Parent A. 1995. Distribution of limbic system-associated membrane protein immunoreactivity in primate basal ganglia. Neuroscience 69:71–81.

Côté PY, Levitt P, Parent A. 1996. Limbic system-associated membrane protein (LAMP) in primate amygdala and hippocampus. Hippocampus 6:483–494.

Cuello AC, Galfre G, Milstein C. 1979. Detection of substance P in the central nervous system by a monoclonal antibody. Proc Natl Acad Sci USA 76:3532–3536.

Daunais JB, Letchworth SR, Sim-Selley LJ, Smith HR, Childers SR, Porrino LJ. 2001. Functional and anatomical localization of mu opioid receptors in the striatum, amygdala, and extended amygdala of the nonhuman primate. J Comp Neurol 433:471–485.

Davis M, Shi C. 1999. The extended amygdala: are the central nucleus of the amygdala and the bed nucleus of the stria terminalis differentially involved in fear versus anxiety? Ann N Y Acad Sci 877:281–291.

de Olmos JS, Alheid GF, Beltramino CA. 1985. Amygdala. In: Paxinos G, editor. The rat nervous system. Sydney: Academic Press. p 223–234.

de Lacalle S, Saper CB. 1997. The cholinergic system in the primate brain: Basal forebrain and pontine-tegmental groups. In: Bloom FE, Björklund A, Hökflet T, editors. Handbook of chemical neuroanatomy. Vol 13, the primate nervous system, part 1. Amsterdam: Elsevier. p 217–262.

Druga R, Chen S, Bentivoglio M. 1993. Parvalbumin and calbindin in the rat claustrum: an immunocytochemical study combined with retrograde tracing from frontoparietal cortex. J Chem Neuroanat 6:399–406.

Eblen F, Graybiel AM. 1995. Highly restricted origin of prefrontal cortical inputs to striosomes in the macaque monkey. J Neurosci 15:5999–6013.

Elliott R, Friston KJ, Dolan RJ. 2000. Dissociable neural responses in human reward systems. J Neurosci 20:6159–6165.

Friedman DP, Aggleton JP, Saunders RC. 2002. Comparison of hippocampal, amygdala, and perirhinal projections to the nucleus accumbens:

combined anterograde and retrograde tracing study in the macaque brain. J Comp Neurol 450:345–365.

Fudge JL, Kunishio K, Walsh P, Richard C, Haber SN. 2002. Amygdaloid projections to ventromedial striatal subterritories in the primate. Neuroscience 110:257–275.

Geneser-Jensen FA, Blackstad TW. 1971. Distribution of acetyl cholinesterase in the hippocampal region of the guinea pig. I. Entorhinal area, parasubiculum, and presubiculum. Z Zellforsch Mikrosk Anat 114: 460–481.

Geula C, Tokuno H, Hersh L, Mesulam MM. 1990. Human striatal cholinergic neurons in development, aging and Alzheimer's disease. Brain Res 508:310–312.

Geula C, Schatz CR, Mesulam MM. 1993. Differential localization of NADPH-diaphorase and calbindin-D28k within the cholinergic neurons of the basal forebrain, striatum and brainstem in the rat, monkey, baboon and human. Neuroscience 54:461–476.

Groenewegen HJ, Russchen FT. 1984. Organization of the efferent projections of the nucleus accumbens to pallidal, hypothalamic, and mesencephalic structures: a tracing and immunohistochemical study in the cat. J Comp Neurol 223:347–367.

Groenewegen HJ, Berendse HW, Wolters JG, Lohman AH. 1990. The anatomical relationship of the prefrontal cortex with the striatopallidal system, the thalamus and the amygdala: evidence for a parallel organization. Prog Brain Res 85:95–116.

Groenewegen HJ, Berendse HW, Meredith GE, Haber SN, Voorn P, Wolters JG, Lohman AH. 1991. Functional anatomy of the ventral, limbic system-innervated striatum. In: Willner P, Scheel-Kruger J, editors. The mesolimbic dopamine system: from motivation to action. Chichester: John Wiley and Sons. p 19–60.

Groenewegen HJ, Wright CI, Beijer AV. 1996. The nucleus accumbens: gateway for limbic structures to reach the motor system? Prog Brain Res 107:485–511.

Grosman DD, Lorenzi MV, Trinidad AC, Strauss WL. 1995. The human choline acetyltransferase gene encodes two proteins. J Neurochem 65:484–491.

Haber SN, McFarland NR. 1999. The concept of the ventral striatum in nonhuman primates. Ann N Y Acad Sci 877:33–48.

Haber SN, Wolfe DP, Groenewegen HJ. 1990. The relationship between ventral striatal efferent fibers and the distribution of peptide-positive woolly fibers in the forebrain of the rhesus monkey. Neuroscience 39:323–338.

Haber SN, Kunishio K, Mizobuchi M, Lynd-Balta E. 1995. The orbital and medial prefrontal circuit through the primate basal ganglia. J Neurosci 15:4851–4867.

Haber SN, Fudge JL, McFarland NR. 2000. Striatonigrostriatal pathways in primates form an ascending spiral from the shell to the dorsolateral striatum. J Neurosci 20:2369–2382.

Heimer L. 2000. Basal forebrain in the context of schizophrenia. Brain Res Rev 31:205–235.

Heimer L, Alheid GF. 1991. Piecing together the puzzle of the basal forebrain anatomy. In: Napier TC, Kalivas PW, Hanin I, editors. The basal forebrain. New York: Plenum Press. p 1–42.

Heimer L, Wilson RD. 1975. The subcortical projections of allocortex: similarities in the neuronal associations of the hippocampus, the piriform cortex and the neocortex. In Santini M, editor. Golgi centennial symposium. New York: Raven Press. p 177–193.

Heimer L, Zahm DS, Churchill L, Kalivas PW, Wohltmann C. 1991. Specificity in the projection patterns of accumbal core and shell in the rat. Neuroscience 41:89–125.

Heimer L, de Olmos JS, Alheid GF, Pearson J, Sakamoto N, Shinoda K, Marksteiner J, Switzer RC III. 1999. The human basal forebrain. Part II. In: Bloom FE, Björklund A, Hökflet T, editors. Handbook of chemical neuroanatomy. Vol 15, the primate nervous system, part 3. Amsterdam: Elsevier. p 57–226.

Holt DJ, Hersh LB, Saper CB. 1996. Cholinergic innervation in the human striatum: a three-compartment model. Neuroscience 74:67–87.

Holt DJ, Graybiel AM, Saper CB. 1997. Neurochemical architecture of the human striatum. J Comp Neurol 384:1–25.

Hussain Z, Johnson LR, Totterdell S. 1996. A light and electron microscopic study of NADPH-diaphorase-, calretinin- and parvalbumin-containing neurons in the rat nucleus accumbens. J Chem Neuroanat 10:19–39.

Ichitani Y, Tanaka M, Okamura H, Ibata Y. 1993. Cholinergic neurons contain calbindin-D28k in the monkey medial septal nucleus and nucleus of the diagonal band: an immunocytochemical study. Brain Res 625:328–332.

Ikemoto S. 2002. Ventral striatal anatomy of locomotor activity induced by cocaine, D-amphetamine, dopamine and D1/D2 agonists. Neuroscience 113:939–955.

Ikemoto K, Satoh K, Maeda T, Fibiger HC. 1995. Neurochemical heterogeneity of the primate nucleus accumbens. Exp Brain Res 104:177–190.

Ikemoto K, Kitahama K, Maeda T, Satoh K. 1996. The distribution of noradrenaline, serotonin and gamma-aminobutyric acid in the monkey nucleus accumbens. Prog Neuropsychopharmacol Biol Psychiatry 20: 1403–1412.

Johnston JB. 1923. Further contributions to the study of the evolution of the forebrain. J Comp Neurol 35:337–481.

Jongen-Relo AL, Groenewegen HJ, Voorn P. 1993. Evidence for a multicompartmental histochemical organization of the nucleus accumbens in the rat. J Comp Neurol 337:267–276.

Jongen-Relo AL, Voorn P, Groenewegen HJ. 1994. Immunohistochemical characterization of the shell and core territories of the nucleus accumbens in the rat. Eur J Neurosci 6:1255–1264.

Keller F, Rimvall K, Barbe MF, Levitt P. 1989. A membrane glycoprotein associated with the limbic system mediates the formation of the septohippocampal pathway in vitro. Neuron 3:551–561.

Kelley AE. 1999. Functional specificity of ventral striatal compartments in appetitive behaviors. Ann N Y Acad Sci 877:71–90.

Kelley AE, Domesick VB. 1982. The distribution of the projection from the hippocampal formation to the nucleus accumbens in the rat: an anterograde- and retrograde-horseradish peroxidase study. Neuroscience 7:2321–2335.

Kelley AE, Domesick VB, Nauta WJ. 1982. The amygdalostriatal projection in the rat—an anatomical study by anterograde and retrograde tracing methods. Neuroscience 7:615-630.

Kiss J, Magloczky Z, Somogyi J, Freund TF. 1997. Distribution of calretinin-containing neurons relative to other neurochemically identified cell types in the medial septum of the rat. Neuroscience 78:399–410.

Koob GF. 1992. Drugs of abuse: anatomy, pharmacology and function of reward pathways. Trends Pharmacol Sci 13:177–184.

Koob GF. 1999. The role of the striatopallidal and extended amygdala systems in drug addiction. Ann N Y Acad Sci 877:445–460.

Koob GF, Robledo P, Markou A, Caine SB. 1993. The mesolimbic circuit in drug dependence and reward—a role for the extended amygdala? In: Kalivas PW, Barnes CD, editors. Limbic motor circuits and neuropsychiatry. Boca Raton, FL: CRC Press. p 289–309.

Landwehrmeyer B, Mengod G, Palacios JM. 1993. Dopamine D3 receptor mRNA and binding sites in human brain. Brain Res Mol Brain Res 18:187–192.

Lauer M, Heinsen H. 1996. Cytoarchitectonics of the human nucleus accumbens. J Hirnforsch 37:243–254.

Lehericy S, Hirsch EC, Cervera P, Hersh LB, Hauw JJ, Ruberg M, Agid Y. 1989. Selective loss of cholinergic neurons in the ventral striatum of patients with Alzheimer disease. Proc Natl Acad Sci USA 86:8580–8584.

Levitt P. 1984. A monoclonal antibody to limbic system neurons. Science 223:299–301.

Majak K, Pikkarainen M, Kemppainen S, Jolkkonen E, Pitkanen A. 2002. Projections from the amygdaloid complex to the claustrum and the endopiriform nucleus: a *Phaseolus vulgaris* leucoagglutinin study in the rat. J Comp Neurol 451:236–249.

Martin LJ, Hadfield MG, Dellovade TL, Price DL. 1991. The striatal mosaic in primates: patterns of neuropeptide immunoreactivity differentiate the ventral striatum from the dorsal striatum. Neuroscience 43:397–417.

McDonald AJ. 1991. Topographical organization of amygdaloid projections to the caudatoputamen, nucleus accumbens, and related striatal-like areas of the rat brain. Neuroscience 44:15–33.

Meredith GE, Blank B, Groenewegen HJ. 1989. The distribution and compartmental organization of the cholinergic neurons in nucleus accumbens of the rat. Neuroscience 31:327–345.

Meredith GE, Agolia R, Arts MP, Groenewegen HJ, Zahm DS. 1992. Morphological differences between projection neurons of the core and shell in the nucleus accumbens of the rat. Neuroscience 50:149–162.

Meredith GE, Pennartz CM, Groenewegen HJ. 1993. The cellular framework for chemical signalling in the nucleus accumbens. Prog Brain Res 99:3–24.

Meredith GE, Pattiselanno A, Groenewegen HJ, Haber SN. 1996. Shell and core in monkey and human nucleus accumbens identified with antibodies to calbindin-D28k. J Comp Neurol 365:628–639.

Mesulam MM. 1985. Patterns in behavioral neuroanatomy: Association areas, the limbic system, and hemispheric specialization. In: Plum F, Baringer JR, Gilman S, editors. Principles of behavioral neurology. Philadelphia: Davis. p 1–192.

Mesulam MM, Mufson EJ, Wainer BH, Levey AI. 1983. Central cholinergic pathways in the rat: an overview based on an alternative nomenclature (Ch1–Ch6). Neuroscience 10:1185–1201.

Mesulam MM, Mufson EJ, Levey AI, Wainer BH. 1984. Atlas of cholinergic neurons in the forebrain and upper brainstem of the macaque based on monoclonal choline acetyltransferase immunohistochemistry and acetylcholinesterase histochemistry. Neuroscience 12:669–686.

Meyer G, Gonzalez-Hernandez T, Carrillo-Padilla F, Ferres-Torres R. 1989. Aggregations of granule cells in the basal forebrain (islands of Calleja): Golgi and cytoarchitectonic study in different mammals, including man. J Comp Neurol 284:405–428.

Moga MM, Weis RP, Moore RY. 1995. Efferent projections of the paraventricular thalamic nucleus in the rat. J Comp Neurol 359:221–238.

Mogenson GJ, Yang CR. 1991. The contribution of basal forebrain to limbic-motor integration and the mediation of motivation to action. Adv Exp Med Biol 295:267–290.

Mogenson GJ, Jones DL, Yim CY. 1980. From motivation to action: functional interface between the limbic system and the motor system. Prog Neurobiol 14:69–97.

Mogenson GJ, Brudzynski SM, Wu M, Yang CR, Yim CCY. 1993. From motivation to action: a review of dopaminergic regulation of limbic-nucleus accumbens-ventral pallidum-pedunculopontine nucleus circuitries involved in limbic-motor integration. In: Kalivas PW, Barnes CD, editors. Limbic motor circuits and neuropsychiatry. Boca Raton, FL: CRC Press. p 193–236.

Morel A, Loup F, Magnin M, Jeanmonod D. 2002. Neurochemical organization of the human basal ganglia: anatomofunctional territories defined by the distributions of calcium-binding proteins and SMI-32. J Comp Neurol 443:86–103.

Murray AM, Ryoo HL, Gurevich E, Joyce JN. 1994. Localization of dopamine D3 receptors to mesolimbic and D2 receptors to mesostriatal regions of human forebrain. Proc Natl Acad Sci USA 91:11271–11275.

Nauta WJ, Smith GP, Faull RL, Domesick VB. 1978. Efferent connections and nigral afferents of the nucleus accumbens septi in the rat. Neuroscience 3:385–401.

Phelps PE, Vaughn JE. 1986. Immunocytochemical localization of choline acetyltransferase in rat ventral striatum: a light and electron microscopic study. J Neurocytol 15:595–617.

Phillipson OT, Griffiths AC. 1985. The topographic order of inputs to nucleus accumbens in the rat. Neuroscience 16:275–296.

Pioro EP, Mai JK, Cuello AC. 1990. Distribution of substance P- and enkephalin-immunoreactive neurons and fibers. In: Paxinos G, editor. The human nervous system. San Diego: Academic Press. p 1051–1094.

Prensa L, Gimenez-Amaya JM, Parent A. 1999. Chemical heterogeneity of the striosomal compartment in the human striatum. J Comp Neurol 413:603–618.

Resibois A, Rogers JH. 1992. Calretinin in rat brain: an immunohistochemical study. Neuroscience 46:101–134.

Reynhout K, Baizer JS. 1999. Immunoreactivity for calcium-binding proteins in the claustrum of the monkey. Anat Embryol 199:75–83.

Reynolds SM, Berridge KC. 2001. Fear and feeding in the nucleus accumbens shell: rostrocaudal segregation of GABA-elicited, defensive behavior versus eating behavior. J Neurosci 21:3261–3270.

Robbins TW, Everitt BJ. 1996. Neurobehavioral mechanism of reward and motivation. Curr Opin Neurobiol 6:228–236.

Russchen FT, Bakst I, Amaral DG, Price JL. 1985. The amygdalostriatal projections in the monkey. An anterograde tracing study. Brain Res 329:241–257.

Sakamoto N, Pearson J, Shinoda K, Alheid GF, de Olmos JS, Heimer L. 1999. The human basal forebrain. Part II. An overview. In: Bloom, FE, Björklund A, Hökfelt T, editors. Handbook of chemical neuroanatomy. Vol 15, the primate nervous system, part 3. Amsterdam: Elsevier. p 1–57.

Sanides F. 1957. Die Insulae terminales des Erwachsenen Gehirns des Menschen. J Hirnforsch 3:244–273.

Schultz W, Apicella P, Scarnati E, Ljungberg T. 1992. Neuronal activity in monkey ventral striatum related to the expectation of reward. J Neurosci 12:4595–4610.

Schultz WP, Dayan P, Montague PR. 1997. A neural substrate of prediction and reward. Science 275:1593–1599.

Schwaller B, Buchwald P, Blumcke I, Celio MR, Hunziker W. 1993. Characterization of a polyclonal antiserum against the purified human recombinant calcium binding protein calretinin. Cell Calcium 14:639–648.

Seifert U, Hartig W, Grosche J, Bruckner G, Riedel A, Brauer K. 1998. Axonal expression sites of tyrosine hydroxylase-, calretinin- and calbindin-immunoreactivity in striato-pallidal and septal nuclei of the rat brain: a double-immunolabelling study. Brain Res 795:227–246.

Selden N, Geula C, Hersh L, Mesulam MM. 1994. Human striatum: chemoarchitecture of the caudate nucleus, putamen and ventral striatum in health and Alzheimer's disease. Neuroscience 60:621–636.

Sherk H. 1986. The claustrum and the cerebral cortex. In: Jones EG, Peters A, editors. Cerebral cortex. New York: Plenum. p 467–499.

Shima K, Hoshi E, Tanji J. 1996. Neuronal activity in the claustrum of the monkey during performance of multiple movements. J Neurophysiol 76:2115–2119.

Stein EA, Pankiewicz J, Harsch HH, Cho JK, Fuller SA, Hoffmann RG, Hawkins M, Rao SM, Bandettini PA, Bloom AS. 1998. Nicotine-induced limbic cortical activation in the human brain: a functional MRI study. Am J Psychiatry 155:1009–1015.

Talbot K, Woolf NJ, Butcher LL. 1988. Feline islands of Calleja complex: II. Cholinergic and cholinesterasic features. J Comp Neurol 275:580–603.

Vonkeman HE, Voorn P, Brady LS, Berendse HW, Richfield EK. 1996. Opioid receptor ligand binding in the human striatum: II. Heterogeneous distribution of kappa opioid receptor labeled with [^{3}H]bremazocine. J Comp Neurol 374:223–229.

Voorn P, Gerfen CR, Groenewegen HJ. 1989. Compartmental organization of the ventral striatum of the rat: immunohistochemical distribution of enkephalin, substance P, dopamine, and calcium-binding protein. J Comp Neurol 289:189–201.

Voorn P, Brady LS, Schotte A, Berendse HW, Richfield EK. 1994. Evidence for two neurochemical divisions in the human nucleus accumbens. Eur J Neurosci 6:1913–1916.

Voorn P, Brady LS, Berendse HW, Richfield EK. 1996. Densitometrical analysis of opioid receptor ligand binding in the human striatum—I. Distribution of mu opioid receptor defines shell and core of the ventral striatum. Neuroscience 75:777–792.

Wahle P, Meyer G. 1986. The olfactory tubercle of the cat. II. Immunohistochemical compartmentation. Exp Brain Res 62:528–540.

Zaborszky L, Alheid GF, Beinfeld MC, Eiden LE, Heimer L, Palkovits M. 1985. Cholecystokinin innervation of the ventral striatum: a morphological and radioimmunological study. Neuroscience 14:427–453.

Zacco A, Cooper V, Chantler PD, Fisher-Hyland S, Horton HL, Levitt P. 1990. Isolation, biochemical characterization and ultrastructural analysis of the limbic system-associated membrane protein (LAMP), a protein expressed by neurons comprising functional neural circuits. J Neurosci 10:73–90.

Zahm DS. 1999. Functional-anatomical implications of the nucleus accumbens core and shell subterritories. Ann N Y Acad Sci 877:113–128.

Zahm DS, Brog JS. 1992. On the significance of subterritories in the "accumbens" part of the rat ventral striatum. Neuroscience 50:751–767.

Zahm DS, Heimer L. 1988. Ventral striatopallidal parts of the basal ganglia in the rat: I. Neurochemical compartmentation as reflected by the distributions of neurotensin and substance P immunoreactivity. J Comp Neurol 272:516–535.

Zahm DS, Heimer L. 1993. Specificity in the efferent projections of the nucleus accumbens in the rat: comparison of the rostral pole projection patterns with those of the core and shell. J Comp Neurol 327:220–232.